Stem Cell Reports
Article

ISSCR

OPEN ACCESS

IGF-1R Promotes Symmetric Self-Renewal and Migration of Alkaline Phosphatase^{+} Germ Stem Cells through HIF-2α-OCT4/CXCR4 Loop under Hypoxia

Yung-Che Kuo,[1,3,13] Heng-Kien Au,[4,5,6,13] Jue-Liang Hsu,[7] Hsiao-Feng Wang,[1,3] Chiung-Ju Lee,[1,8] Syue-Wei Peng,[1,8] Ssu-Chuan Lai,[1,8] Yu-Chih Wu,[3] Hong-Nerng Ho,[9,10] and Yen-Hua Huang[1,2,3,5,8,11,12,*]

[1]Department of Biochemistry and Molecular Cell Biology, School of Medicine, College of Medicine, Taipei Medical University, 11031 Taipei, Taiwan
[2]International PhD Program for Cell Therapy and Regeneration Medicine, College of Medicine, Taipei Medical University, 11031 Taipei, Taiwan
[3]Center for Cell Therapy and Regeneration Medicine, Taipei Medical University, 11031 Taipei, Taiwan
[4]Department of Obstetrics and Gynecology, School of Medicine, College of Medicine, Taipei Medical University, 11031 Taipei, Taiwan
[5]Center for Reproductive Medicine, Taipei Medical University Hospital, Taipei Medical University, 11031 Taipei, Taiwan
[6]Department of Obstetrics and Gynecology, Taipei Medical University Hospital, 11031 Taipei, Taiwan
[7]Department of Biological Science and Technology, National Pingtung University of Science and Technology, 91201 Pingtung, Taiwan
[8]Graduate Institute of Medical Sciences, College of Medicine, Taipei Medical University, 11031 Taipei, Taiwan
[9]Graduate Institute of Clinical Medicine, College of Medicine, National Taiwan University, 10002 Taipei, Taiwan
[10]Department of Obstetrics and Gynecology, Division of Reproductive Endocrinology and Infertility, National Taiwan University and Hospital, 10041 Taipei, Taiwan
[11]Comprehensive Cancer Center of Taipei Medical University, 10031 Taipei, Taiwan
[12]The Ph.D. Program for Translational Medicine, College of Medical Science and Technology, Taipei Medical University, 10031 Taipei, Taiwan
[13]Co-first author
*Correspondence: rita1204@tmu.edu.tw
https://doi.org/10.1016/j.stemcr.2017.12.003

SUMMARY

Hypoxia cooperates with endocrine signaling to maintain the symmetric self-renewal proliferation and migration of embryonic germline stem cells (GSCs). However, the lack of an appropriate *in vitro* cell model has dramatically hindered the understanding of the mechanism underlying this cooperation. Here, using a serum-free system, we demonstrated that hypoxia significantly induced the GSC mesenchymal transition, increased the expression levels of the pluripotent transcription factor OCT4 and migration-associated proteins (SDF-1, CXCR4, IGF-1, and IGF-1R), and activated the cellular expression and translocalization of the CXCR4-downstream proteins ARP3/pFAK. The underlying mechanism involved significant IGF-1/IGF-1R activation of OCT4/CXCR4 expression through HIF-2α regulation. Picropodophyllin-induced inhibition of IGF-1R phosphorylation significantly suppressed hypoxia-induced SDF-1/CXCR4 expression and cell migration. Furthermore, transactivation between IGF-1R and CXCR4 was involved. In summary, we demonstrated that niche hypoxia synergistically cooperates with its associated IGF-1R signaling to regulate the symmetric division (self-renewal proliferation) and cell migration of alkaline phosphatase-positive GSCs through HIF-2α-OCT4/CXCR4 during embryogenesis.

INTRODUCTION

Germline stem cells (GSCs) are responsible for gamete formation and genetic transmission. During embryogenesis, GSCs include embryonic gamete precursor primordial germ cells (PGCs), gonocytes (postmigratory PGCs), and spermatogonial stem cells (SSCs). PGCs are the earliest population of germ cells derived from proximal epiblast cells at around embryonic day 7.25 (E7.25) (Ginsburg et al., 1990; McLaren, 2003). Internal gene regulation and an external niche signal are critical factors for PGC development. Internal transcription factors such as FRAGILIS, STELLA, and BLIMP1 initiate the emergence of PGCs (Ohinata et al., 2005; Saitou et al., 2002), followed by the external BMP4 signal, to enable PGC competence (Lawson et al., 1999; Ying et al., 2001). When PGCs are competent, they express strong alkaline phosphatase (AP) activity and migrate from the hindgut to the embryonic genital ridges at E10–E11.5 (McLaren, 2003; Saga, 2008). Deregulation of the symmetric self-renewal proliferation and/or migration of PGCs leads to an insufficient number of germ cells in embryonic gonads, resulting in infertility and increasing the risk of extragonadal germ cell tumors (Hoei-Hansen et al., 2006).

Physiological niche hypoxia plays critical roles in germ cell development during embryogenesis (Covello et al., 2006; Fischer and Bavister, 1993; Forristal et al., 2010; Simon and Keith, 2008). Niche hypoxia stabilizes hypoxia-inducible factors (HIFs) by preventing their interaction with pVHL and ubiquitination/proteasomal degradation (Ginouvés et al., 2008; Haase, 2009). HIF-2α is coincidently expressed with the pluripotent transcription factor OCT4 in multiple embryonic tissues, such as blastocyst-stage embryos, E7.5 embryos, and PGCs. Loss of HIF-2α considerably reduces the number of embryonic PGCs in the genital ridge (Covello et al., 2006), and leads to azoospermia (Scortegagna et al., 2003), demonstrating that HIF-2α expression is required for PGC development.

In addition to niche hypoxia, its associated external endocrine signaling is crucial. Studies have suggested some factors involved in PGC migration toward the

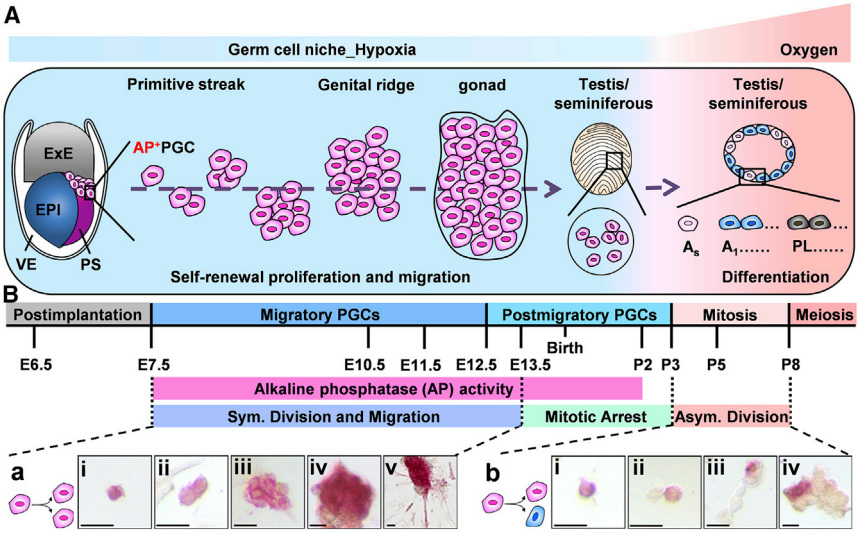

Figure 1. Schematic Diagram of Mouse Postimplantation Germ Cell Development in Symmetric Self-Renewal Proliferation and Migration

(A) Germ cell development profile under different oxygen tension conditions during embryogenesis.

(B) Germ cell developmental profile. (a and b) AP staining (in red). (a) i–iv: symmetric self-renewal division (Sym.) of AP$^+$GSCs. v: partial migratory AP$^+$GSCs under embryonic hypoxia. (b) i–iv: asymmetric division (Asym.) of AP$^+$GSCs. AP, alkaline phosphatase; ExE, extraembryonic ectoderm; EPI, epiblast; PS, primitive streak; VE, visceral endoderm; AP$^+$PGCs, PGCs with AP activity (in red); A_s, undifferentiated A single spermatogonia; A_1, differentiating A_1 spermatogonia; PL, preleptotene spermatocytes; E, embryonic day; P, postnatal day. Scale bars, 25 μm. See also Figure S3.

genital ridges, and they include STEEL and c-KIT (Raz, 2004), stromal cell-derived factor 1 (SDF-1), and C-X-C chemokine receptor 4 (CXCR4) (Doitsidou et al., 2002; Molyneaux et al., 2003), transforming growth factor β (Chuva de Sousa Lopes et al., 2005), integrin β1 (Anderson et al., 1999), and RGS14A (Hartwig et al., 2014), etc. In support, our previous study demonstrated a hypoxia-endocrine insulin-like growth factor 1 (IGF-1) receptor (IGF-1R)-HIF-2α signaling loop for the maintenance of OCT4 and cell proliferation of AP$^+$GSCs (Huang et al., 2014). These observations highlight the potential role of IGF-1R in proliferation, survival, and cell migration in pluripotent germ cells.

Our limited understanding of niche hypoxia and its associated endocrine signals in germ cell development may be due to the absence of an appropriate *in vitro* stem cell model. The common use of serum-containing culture medium not only considerably reduces cell stemness (Barnes and Sato, 1980; Huang et al., 2009), but also severely interferes with the identification of potential endocrine factors that control germ stem cell fate. In this regard, we previously established an *in vitro* serum-free culture system to generate AP$^+$PGC-like pluripotent stem cells from a wild-type neonatal mouse testis. This serum-free culture system provides a powerful platform for investigating how the signal network of a hypoxic niche affects the migration of pluripotent GSCs. We thus identified a vital role of an IGF-1-dependent pathway in the maintenance of germ cell pluripotency (Huang et al., 2009), and further demonstrated a regulatory IGF-1R-HIF-2α signaling loop in the proliferation and OCT4 maintenance of PGC-like AP$^+$GSCs under hypoxia (Huang et al., 2014). In the present study, we used the serum-free culture system to demonstrate that the hypoxic condition cooperates with endocrine IGF-1R signaling to promote early germ cell migration through the HIF-2α-CXCR4 regulatory loop. The findings of our studies can elucidate underlying molecular mechanisms between niche hypoxia and its associated endocrine signaling for early germ cell symmetric self-renewal proliferation and migration during embryogenesis.

RESULTS

Symmetric Self-Renewal Proliferation and Migration for Early Germ Cell Development under an Embryonic Hypoxic Niche

In early germ cell development, the PGCs derived from proximal epiblast cells form a cluster of AP$^+$ cells underlie the posterior part of the primitive streak at around E7.5. Subsequently, the PGCs undergo self-renewal proliferation (symmetric division) and migration, pass through the hindgut, then move to the embryonic genital ridges at E10–E11.5, and arrive at the gonad at E12.5. In males, the gonad then develops to the testis; at this stage, the germ cells are located in the lumen of the seminiferous tubule of the testis and halt proliferation, staying in the G0 phase until postnatal day 3 (P3) (postmigratory PGCs). All the germ cells from the primitive streak to the genital ridge (migratory PGCs) are under a physiological hypoxic niche (E7.5–P2; Figure 1A) (Free et al., 1976). During this migration process, these embryonic germ cells present strong AP activity and undergo self-renewal proliferation to

increase the germ cell number from approximately 100 to 20,000 cells (Brinster, 2002). After P3, the GSCs home in on the testicular basal membrane to respond to niche oxygen, reduce AP activity, and undergo asymmetric division (both of self-renewal and differentiation). The GSCs differentiate into A single (A_s) cells and undergo mitosis into A_1 spermatogonia (P5), followed by meiosis (after P8; Figure 1A).

Because the GSCs of P2 neonatal mouse testis have gonocyte character, we previously generated pluripotent AP$^+$GSCs derived from P2 neonatal mouse testis (AP$^+$GSCs) using a serum-free culture condition (Huang et al., 2009). The AP$^+$GSCs expressed a CD49f cell surface marker, and had PGC-related pluripotency *in vitro* and *in vivo* (Huang et al., 2009, 2014). By using this PGC-like AP$^+$GSC cell platform, symmetric (Figure 1B-a) and asymmetric division (Figure 1Bb) was employed to mimic embryonic germ cell development.

Hypoxia-Induced Symmetric Self-Renewal Proliferation and Mesenchymal-Like Morphological Change in CD49f$^+$AP$^+$GSCs

Oxygen tension appears to be highly linked to stem cell self-renewal, differentiation, and migration. The interaction between niche hypoxia and its associated endocrine signaling apparently plays a critical role. To examine the effect of oxygen tension on embryonic germ cells, the AP$^+$GSCs were cultivated in serum-free medium under different oxygen tension conditions.

As shown in Figure 2, hypoxic conditions (5% or 3% O_2) significantly increased the AP$^+$GSC colony size and AP activity compared with normoxic condition (21% O_2; Figures 2Ab and 2Ac versus 2Aa). We discovered that 5% oxygen tension significantly increased colony number and size in AP$^+$GSCs (Figure 2B). Decreasing the oxygen concentration to 1%, which is similar to the embryonic hypoxic environment, significantly induced the cell into an adherent cluster mesenchymal-like morphology, indicating the effect of hypoxia on cell migration activation (Figures 2Ad and S1). Further switching the AP$^+$GSCs from 1% O_2 to 5% O_2 culture conditions for 7 days led to a significant re-formation of GSC colonies and an increased colony size (Figure S1B).

The effect of hypoxia on AP$^+$GSC symmetric self-renewal proliferation was further supported by the results of a bromodeoxyuridine incorporation assay (Figure 2C); in particular, the AP$^+$GSCs exhibited migratory activity under hypoxic condition (arrowhead, Figures 2Cb and 2Cc). The percentage of GSC colonies with migrating GSC cells under different levels of oxygen tension is shown in Figure 2D. These results strongly highlight the effect of embryonic hypoxia on the self-renewal proliferation and cell migration of AP$^+$GSCs.

The differential protein secretion profiles of AP$^+$GSCs under normoxia and hypoxia were further examined by liquid chromatography tandem-mass spectrometry (LC-MS/MS). Figure 2E illustrates the gene ontology (GO) results for the cellular component analysis. We found a dramatic increase in the expression levels of extracellular matrix- and extracellular region-associated proteins in AP$^+$GSCs under the 5% O_2 hypoxic condition (Figure 2Ea). Further analysis showed a dominant increase in protein classes associated with the cytoskeleton, extracellular matrix, hydrolase, nucleic acid binding, and receptors (Figure 2Eb). Among them, 13 protein classes of restricted hypoxic AP$^+$GSCs were markedly upregulated (Table S1), with few occupying more than 10% of the total proteins including the classes of the extracellular matrix and receptor (Figure 2Eb). The hypoxia-associated signaling pathways involved cell growth (HIF, cell-cycle, DNA replication, insulin/IGF, phosphatidylinositol 3-kinase [PI3K], and JAK/STAT), migration (HIF and integrin), and stemness (epidermal growth factor, fibroblast growth factor, Hedgehog, HIF, insulin/IGF, integrin, JAK/STAT, and PI3K; Figure 2Ec).

The secretome analysis of hypoxic AP$^+$GSCs indicated that the hypoxic condition significantly increased the secretion of crucial proteins (ratio of hypoxia/normoxia), including CXCL12 (SDF-1, 11.6-fold), VEGFA (5.55-fold), MMP2 (5.02-fold), thrombospondin 2 (THBS2) (3.87-fold), and versican (VCAN) (3.32-fold) (Figure 2F; Table S2). The representative LC-MS/MS-determined differentially expressed protein levels of specific target genes under normoxia (21% O_2) and hypoxia (5% O_2) were further confirmed using real-time qRT-PCR analysis (Figure 2G). As the SDF-1 and its receptor CXCR4 are well linked to cell migration (Barriga et al., 2013; Tu et al., 2016), the upregulation of SDF-1 under hypoxia would support the observation of the migratory mesenchymal-like morphological transition of AP$^+$GSCs, by which the migration from the hindgut to the genital ridge during early embryogenesis is initiated. These observations strongly highlight the role of niche hypoxia in the symmetric self-renewal proliferation and migration of early embryonic GSCs.

Hypoxia Increased the Expression of Stemness- and Migration-Associated Proteins Involving the CXCR4 Signal in PGC-Like CD49f$^+$AP$^+$GSCs

We have previously identified CD49f as a cell surface marker of AP$^+$GSCs (Huang et al., 2009, 2014). To further examine the effect of niche hypoxia on AP$^+$GSC signal regulation, the CD49f$^+$AP$^+$GSCs were isolated using a magnetic-activated cell-sorting system (MACS), and the PGC-like characters were confirmed by genetic and epigenetic analyses. We found that the MACS purification

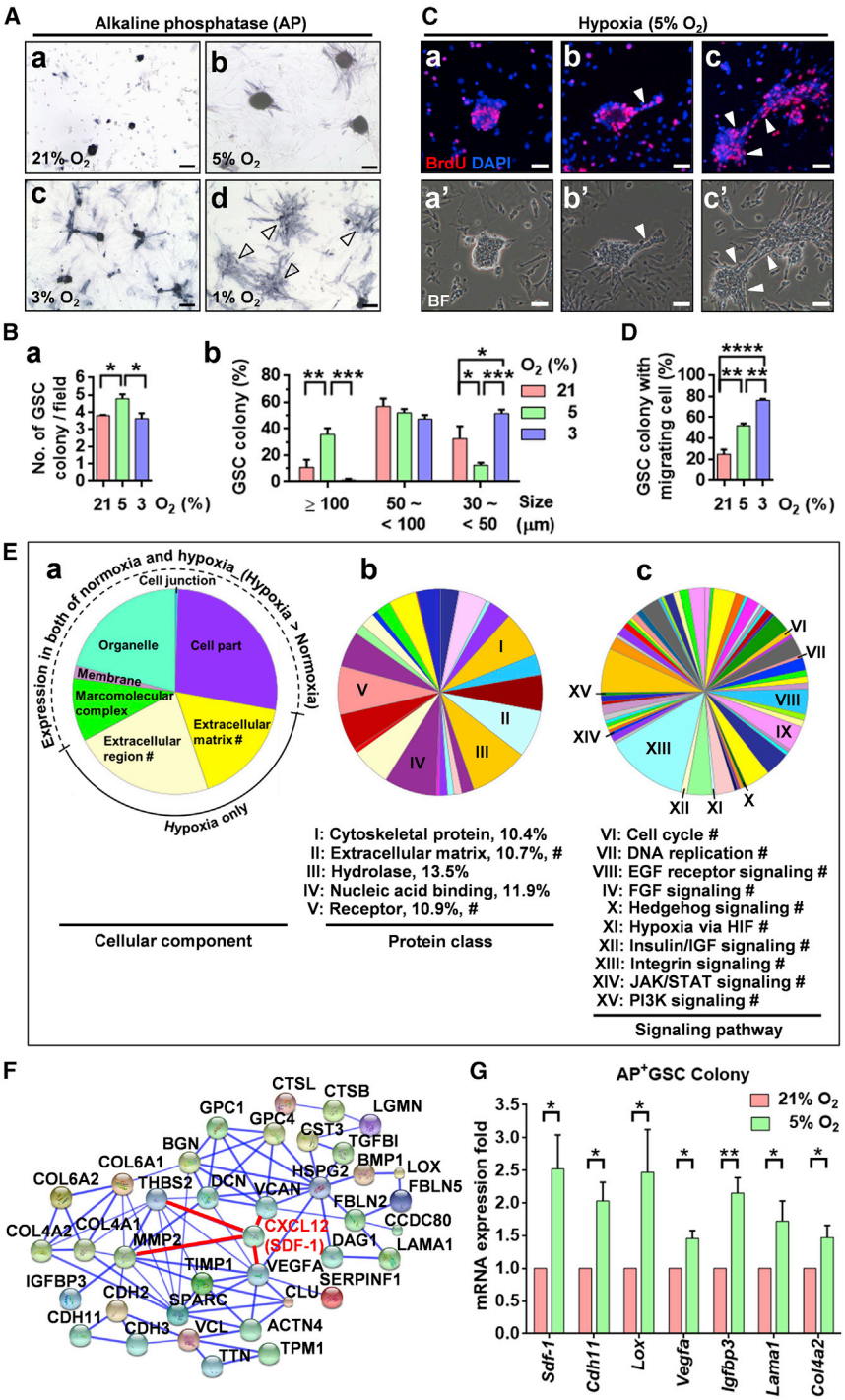

Figure 2. Effect of Oxygen Tension on AP$^+$GSCs in a Serum-Free Culture System

(A) Colony morphology and AP activity (in blue) of mouse AP$^+$GSCs under normoxia (21% O_2) and hypoxia (5% and 3% O_2). Cluster of mesenchymal-like cells under 1% O_2 hypoxia (arrowhead). Scale bar, 100 μm.

(B) Quantification of GSC colony number and size distribution. One-way ANOVA.

(C) Bromodeoxyuridine incorporation assay of AP$^+$GSCs under hypoxia (5% O_2). The arrowheads indicate the hypoxic effect on the cell morphological transition to AP$^+$-migrating GSC cells. Scale bars, 100 μm.

(D) Quantification of the percentage of the GSC colony with migratory cells. One-way ANOVA.

(E) Pie charts representing the GO secretome analysis of mouse AP$^+$GSCs under normoxia (21% O_2) and hypoxia (5% O_2). The secretome analysis was performed using LC-MS/MS. #, proteins expressed under hypoxia only. (a) Cellular component. (b) Protein class; classes accounting for more than 10% of the total classes are labeled I–V. (c) Signaling pathway. Intrigued classifications are labeled VI–XV.

(F) Secretome protein network of AP$^+$GSCs under hypoxia. Protein levels that were higher in the hypoxia than in the normoxia are shown.

(G) Validation of the representative LC-MS/MS-determined differentially expressed proteins in an AP$^+$GSC colony using qRT-PCR. Student's t test. For all quantifications, data are the means ± SEM of at least three independent experiments. *$p < 0.05$, **$p < 0.01$, ***$p < 0.001$, ****$p < 0.0001$. See also Figure S1 and Tables S1–S4.

enriched the CD49f$^+$ cell population by up to 98.55% (Figure S2A). We also confirmed that the purified CD49f$^+$AP$^+$GSCs exhibited strong AP activity and expressed germ cell-specific c-KIT (Figures S2B and S2C). The cell identities of CD49f$^+$AP$^+$GSCs were further identified by comparing them with the PGCs (PGC colonies generated from E11.5 embryo gonad) and AP$^+$GSCs (AP$^+$GSC colonies generated from P2 testis) regarding AP activity and transcriptomic and epigenetic analyses. As shown in Figure 3A, all three cell groups had strong AP activity (Figures 3A and S2B). The transcriptomic analysis revealed that the CD49f$^+$AP$^+$GSCs had 531 similar genes

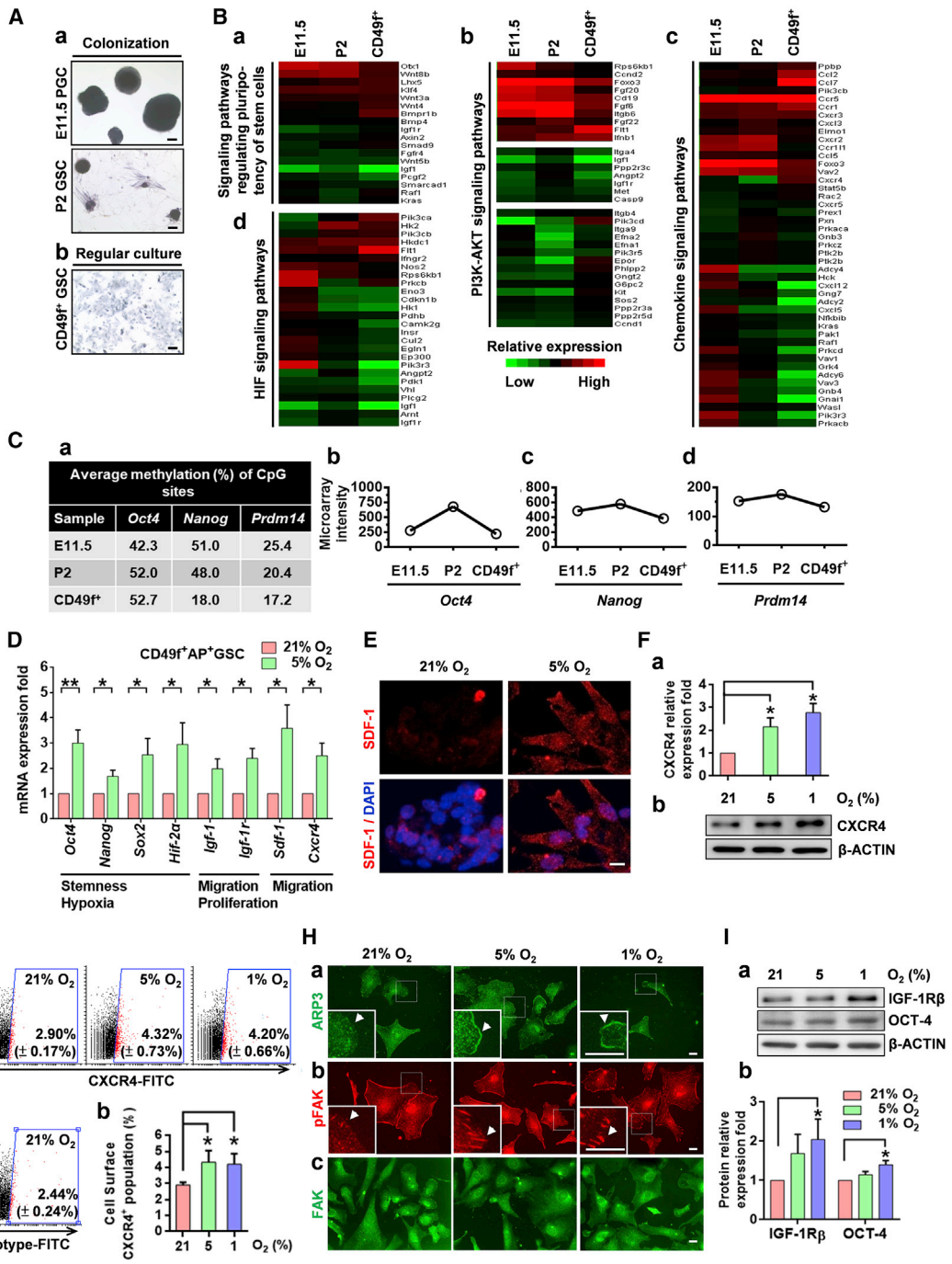

Figure 3. Hypoxia Increased the Expression Levels of Stemness/Migration-Related Proteins in PGC-Like CD49f$^+$AP$^+$GSCs

(A) AP staining (in blue). (a) Colony formation of E11.5 PGCs and P2 GSCs under 5% O_2 hypoxia. (b) Regular culture of purified CD49f$^+$GSCs. Scale bars, 100 μm.

(B) Heatmap of selected gene expression patterns in E11.5 PGCs, P2 GSCs, and purified CD49f$^+$GSCs. Signaling pathways of GO for (a) regulating the pluripotency of stem cells, (b) PI3K-AKT, (c) chemokine, and (d) HIF.

(C) (a) Bisulfite genomic sequencing. (b–d) Gene expression of *Oct4*, *Nanog*, and *Prdm14* in E11.5 PGCs, P2 GSCs, and purified CD49f$^+$GSCs.

(D) The mRNA levels of stemness-, hypoxia-, proliferation-, and migration-related genes of CD49f$^+$AP$^+$GSCs under different oxygen concentrations (qRT-PCR analysis). Student's t test.

(E) Immunofluorescence staining of SDF-1 in CD49f$^+$AP$^+$GSCs under 21% and 5% O_2. Scale bar, 10 μm.

(legend continued on next page)

to the E11.5 PGCs and P2 AP$^+$GSCs, out of a total of 1,400 genes (Figure S3A). Further GO analysis demonstrated that the E11.5 PGCs, P2 GSCs, and CD49f$^+$GSCs shared the similar gene expression profile of the pluripotency regulation signaling pathway, PI3K-AKT signaling (Bendall et al., 2007; Ho et al., 2015; Huang et al., 2009, 2014), chemokine signaling (Sugiyama et al., 2006; Chang et al., 2015), and HIF signaling (Covello et al., 2006) (Figures 3B and S3A). An epigenetic analysis demonstrated that the CD49f$^+$AP$^+$GSCs exhibited a highly similar methylated CpG percentage of pluripotency-related genes, including *Oct4, Nanog, Prdm14* (Figure 3C), *Dppa3*, and *Ddx4*, compared with the E11.5 PGCs and P2 AP$^+$GSCs (Figure S3B). In addition, all three germ cell groups demonstrated similar expression intensity in the corresponding microarray data (Figures 3Cb–3Cd, S3Bb, and S3Bc). These results suggested that the CD49f$^+$AP$^+$GSCs could serve as an appropriate *in vitro* cell model to analyze the effect of hypoxia on PGC-like germ cells.

By using this PGC-like cell platform, we demonstrated hypoxia (5% O_2) significantly increased the gene expression panels of stemness-/hypoxia- (*Oct4*, *Nanog*, *Sox2*, and *Hif-2α*), migration-/proliferation- (*Igf-1* and *Igf-1r*), and migration-associated genes (*Sdf-1* and *Cxcr4*) in CD49f$^+$AP$^+$GSCs (Figure 3D). The upregulation of SDF-1 and c-KIT in CD49f$^+$AP$^+$GSCs under hypoxia was further confirmed using immnunostaining (Figures 3E and S4) and western blotting (Figures S5A and S5B).

Hypoxia also increased CXCR4 protein levels in CD49f$^+$AP$^+$GSCs (Figures 3F and 3G). Given that hypoxia increased SDF-1 expression levels, CXCR4 downstream signaling cascade molecules, such as ARP3 and p-FAK (Dang et al., 2013; Turner, 2000), were examined. As shown in Figure 3H, the hypoxia increased the translocation of the ARP3 protein from the cytoplasm to the leading edge (Figure 3H-a) as well as the FAK activation (pFAK) at the focal adhesion sites (Figure 3Hb) of CD49f$^+$AP$^+$GSCs. The total FAK in CD49f$^+$AP$^+$GSCs is illustrated in Figure 3Hc. In addition, the role of FAK in SDF-1-directed downstream signaling under normoxia is also demonstrated (Figure S6). These observations highlight that the hypoxia-induced mesenchymal-like cell morphological change of CD49f$^+$AP$^+$GSCs may involve SDF-1/CXCR4 signal activation.

IGF-1/IGF-1R Promoted Cell Migration and Activated CXCR4 Expression through HIF-2α in CD49f$^+$AP$^+$GSCs under Normoxia

We demonstrated that the hypoxic condition increased IGF-1R and OCT4 levels (Figure 3I), through which HIF-2α regulated AP$^+$GSC stemness (Huang et al., 2014). Given that CXCR4 is regulated by the HIF protein (Staller et al., 2003), we examined whether the increased IGF-1/IGF-1R signaling is involved in CXCR4 expression in GSCs. As shown in Figure 4, we found that IGF-1 dose-dependently increased the cell adhesion of CD49f$^+$AP$^+$GSCs under normoxia (Figure 4A). High-dose IGF-I treatment effectively enhanced the cell membrane protrusions of CD49f$^+$AP$^+$GSCs, highlighting the migration ability of these cells (Figure 4Aa, inset) (DeMali and Burridge, 2003; Le Clainche and Carlier, 2008). Moreover, compared with normoxia, hypoxia markedly increased the cell adhesion percentage from 5% to approximately 30% under the IGF-1-free culture condition (Figure 4Ab versus Figure S7Ab, IGF-1 = 0 ng/mL). IGF-1 treatment significantly and dose-dependently enhanced the cell adhesion percentage up to 20% (under normoxia) and 50% (under hypoxia) (Figure 4Ab versus Figure S7Ab, IGF-1 = 50 ng/mL). These results strongly support the synergistic effect of hypoxia and IGF-1 in germ cell adhesion and migration. The transwell assay further demonstrated a significant and dose-dependent effect of IGF-I on CD49f$^+$AP$^+$GSC migration ability (Figure 4B). Importantly, we found that IGF-1 significantly and dose-dependently increased the protein expression levels of CXCR4, HIF-2α, IGF-1Rβ, and OCT4 in CD49f$^+$AP$^+$GSCs (Figure 4C). Further knock down of endogenous HIF-2α (shHIF-2α) dramatically suppressed not only the IGF-1-induced expression levels of IGF-IR and OCT4 (Huang et al., 2014), but also that of CXCR4 (Figure 4D). These data demonstrate that IGF-1R activation regulates both of the OCT4 and CXCR4 expressions through HIF-2α regulation, thus promoting the symmetric self-renewal proliferation and cell migration of CD49f$^+$AP$^+$GSCs under hypoxia.

(F) Protein levels of CXCR4 under different oxygen concentrations were analyzed through western blotting. The quantification analysis result is shown. One-way ANOVA.

(G) (a) Cell surface levels of CXCR4 of CD49f$^+$AP$^+$GSCs under different oxygen concentrations were analyzed through flow cytometry. The percentage of CXCR4-positive cells (red dot) is shown. (b) Quantitative analysis of (a). One-way ANOVA.

(H) Cellular localization of the migration-related markers (a) ARP3, (b) pFAK, and (c) FAK under different oxygen concentrations. Arrowheads indicate the specific cellular protein localization of ARP3 and pFAK. Scale bars, 20 μm.

(I) (a) Protein levels of IGF-1Rβ and OCT4 under different oxygen concentrations were analyzed using western blotting. (b) Quantification analysis results. One-way ANOVA.

For all quantifications, data are the means ± SEM of at least three independent experiments. *$p < 0.05$, **$p < 0.01$. See also Figures S2–S6 and Tables S3 and S4.

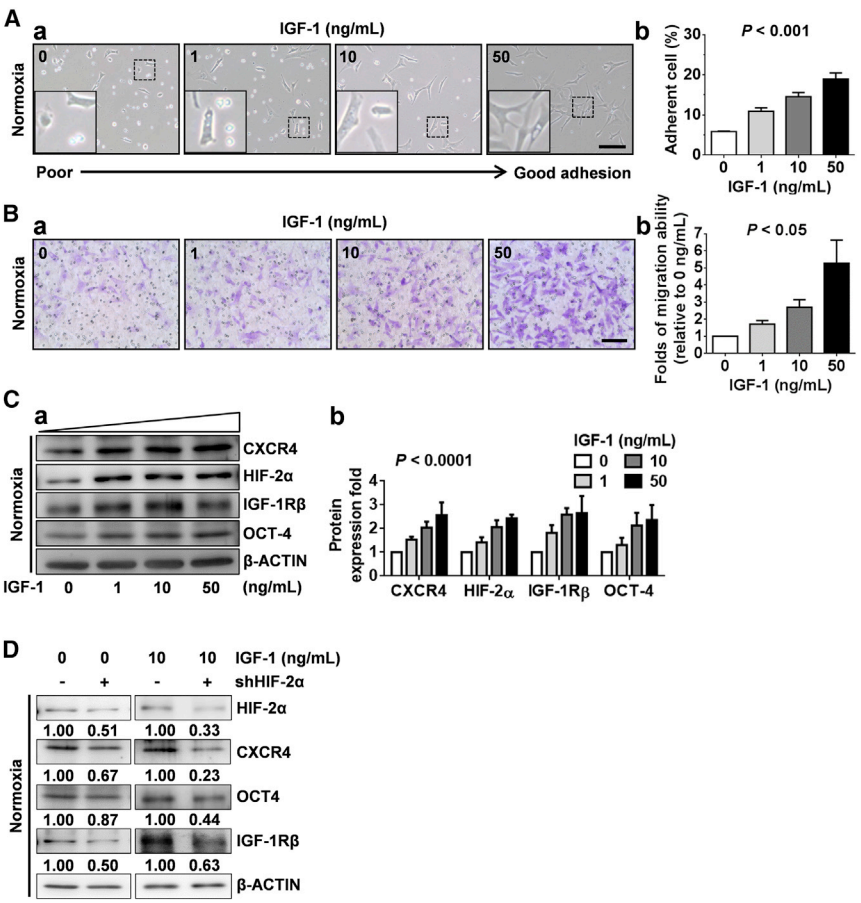

Figure 4. IGF-1 Promoted CXCR4 Expression and Cell Migration through HIF-2α Regulation in CD49f$^+$AP$^+$GSCs

(A) Dose effect of IGF-1 (0, 1, 10, and 50 ng/mL) on the morphology of CD49f$^+$AP$^+$GSC cells. (a) Observation of cell adhesion. Scale bar, 100 μm. (b) Quantitative analysis of (a). $p < 0.001$. One-way ANOVA.

(B) Dose effect of IGF-1 on cell migration. (a) Transwell assay. Scale bar, 100 μm. (b) Quantitative analysis of (a). $p < 0.05$. One-way ANOVA.

(C) Dose effect of IGF-1 on the protein expression levels of CXCR4, HIF-2α, IGF-1Rβ, and OCT4. (a) Western blotting analysis. β-ACTIN served as an internal control. (b) Quantification of (a) was performed and normalized to the corresponding β-ACTIN. $P < 0.0001$. Two-way ANOVA.

(D) Effect of HIF-2α knockdown on the protein levels of CXCR4, OCT4, and IGF-1Rβ in CD49f$^+$AP$^+$GSC cells with or without IGF-1 treatment. Western blotting analysis. The relative quantification was normalized to the corresponding β-ACTIN. For all quantifications, data are the means ± SEM of at least three independent experiments. See also Figure S7.

IGF-1R Activation Mediates Hypoxia-Induced SDF-1/CXCR4 Expression and the Migration of CD49f$^+$AP$^+$GSCs

Because hypoxia significantly induced the expression of SDF-1/CXCR4 and IGF-1/IGF-1R, and that IGF-1 treatment dose-dependently promoted CXCR4 expression and the migration of CD49f$^+$AP$^+$GSCs in the present study, we next examined whether IGF-IR activation regulates the effect of hypoxia on SDF-1 and CXCR4 expression and cell migration. As shown in Figure 5, the IGF-IR phosphorylation inhibitor cyclolignan picropodophyllin (PPP) significantly suppressed hypoxia (1% O_2)-induced SDF-1 (Figure 5A) and cell surface CXCR4 expression (Figure 5B), and suppressed cell migration in CD49f$^+$AP$^+$GSCs, as demonstrated by the transwell assay (Figure 5C). Furthermore, the synergistic effect of hypoxia (1% O_2) and IGF-1/SDF-1 on cell migration (Figures 5D and 5E), as well as cell adhesion (Figure S7A), was demonstrated, and the PPP was discovered to significantly suppress cell migration under hypoxia (Figures 5C–5E and S7B). These results support that IGF-1R activation mediates hypoxia-induced SDF-1/CXCR4 expression and cell migration in CD49f$^+$AP$^+$GSCs.

Crosstalk of IGF-1R and CXCR4 Modulates the Hypoxia-Derived Cell Migration in Mouse CD49f$^+$AP$^+$GSCs

To examine the potential crosstalk of reciprocal transactivation between IGF-1R and CXCR4, CD49f$^+$AP$^+$GSCs were treated with IGF-1 with or without PPP supplementation. Subsequently, the levels of phospho-CXCR4 were examined. We found that IGF-1 effectively stimulated the phosphorylation levels of IGF-1R (pY1135/1136) and AKT (pY473) in 2–5 min. Notably, we found that the levels of p-CXCR4 (pS339) were also slightly but significantly increased after IGF-1 treatment (Figure 6A). A further experiment using the IGF-1R phosphorylation inhibitor PPP revealed that this inhibitor, in addition to effectively suppressing the levels of p-IGF-1R and p-AKT, also significantly suppressed the levels of p-CXCR4 ($p < 0.05$). These results highlight the transactivation of IGF-1R activation on CXCR4 phosphorylation in CD49f$^+$AP$^+$GSCs.

We examined whether SDF-1/CXCR4 signaling transactivated IGF-1R phosphorylation. Figure 6B shows that SDF-1 treatment significantly increased the levels of p-AKT and p-IGF-1R. The CXCR4 signaling inhibitor,

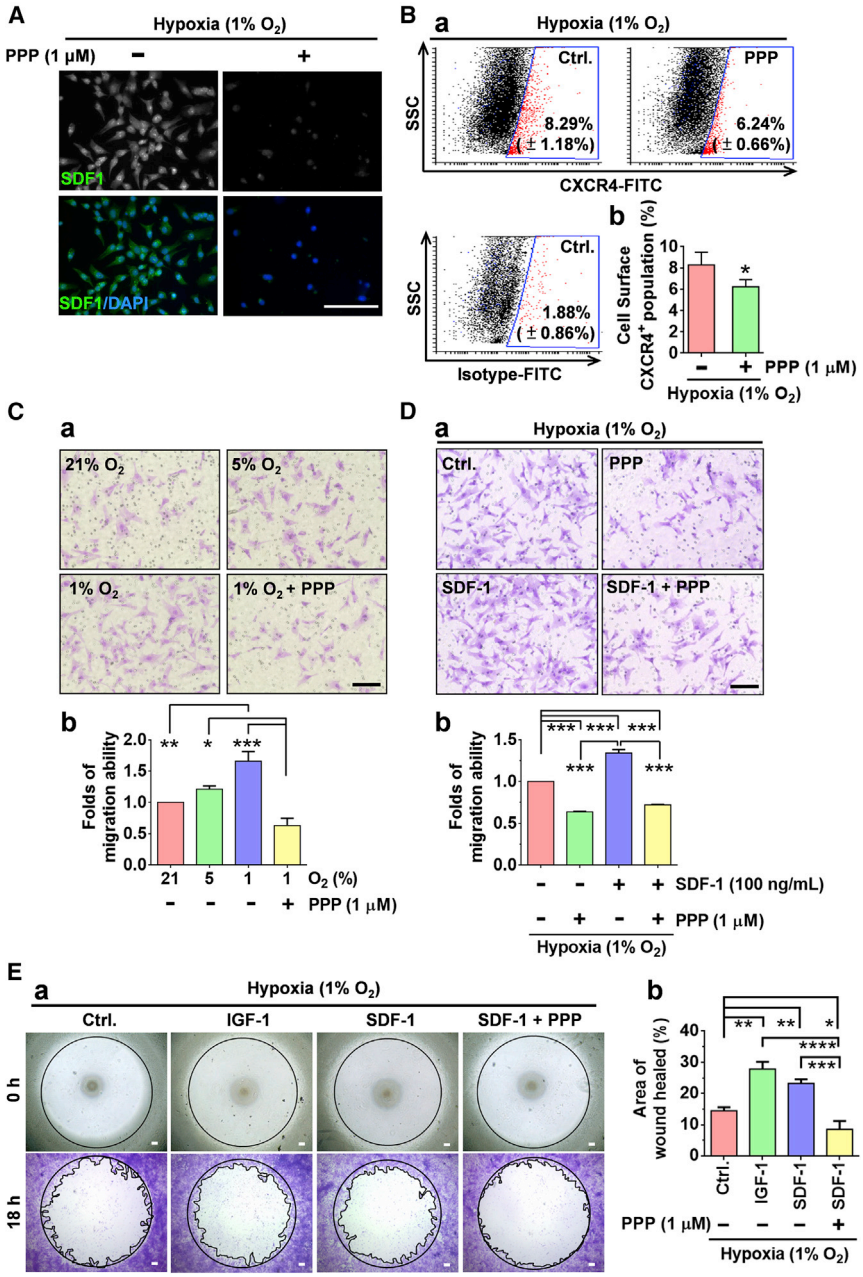

Figure 5. Inhibition of IGF-1R Activation Suppressed Hypoxia-Induced Cell Migration in Mouse CD49f$^+$AP$^+$GSCs

(A) Effect of PPP (IGF-1R phosphorylation inhibitor, 1 μM) on hypoxia (1% O_2)-induced SDF-1 expression in CD49f$^+$AP$^+$GSCs. Immunofluorescence staining. Scale bar, 100 μm.

(B) CXCR4 levels on the surface of CD49f$^+$AP$^+$GSCs with or without PPP treatment under 1% O_2 hypoxia. (a) Dot blots from the flow cytometry analysis. (b) Percentage of CXCR4-positive cells. Student's t test.

(C) Migration ability of CD49f$^+$AP$^+$GSCs under different oxygen concentrations with or without PPP treatment. (a) Transwell assay. Scale bar, 100 μm. (b) Quantitative analysis of (a). One-way ANOVA.

(D) Effect of PPP on SDF-1-induced cell migration under 1% O_2 hypoxia. (a) Transwell assay. Scale bar, 100 μm. (b) Quantitative analysis of (a).

(E) Migration ability of CD49f$^+$AP$^+$GSCs with IGF-1, SDF-1, or PPP treatment for 18 hr under 1% O_2 hypoxia. (a) Wound closure assay. (b) Quantitative analysis of (a). One-way ANOVA. Scale bars, 100 μm.

For all quantifications, data are the means ± SEM of at least three independent experiments. *p < 0.05, **p < 0.01, ***p < 0.001, ****p < 0.0001. See also Figure S7.

AMD3100, effectively suppressed the SDF-1-induced phosphorylation of CXCR4, p-AKT, and the p-IGF-1R (Figure 6B). The crosstalk between IGF-1/IGF-1R and SDF-1/CXCR4 signaling was further supported by the results of the wound closure assay. We discovered that both IGF-1 and SDF-1 significantly increased cell migration ability, and PPP effectively suppressed the effect of SDF-1 on cell migration (Figure 6C). Together with the IGF-1- or hypoxia-induced upregulation of the CXCR4 protein (Figures 3 and 4), these results reveal the crosstalk between IGF-1R and CXCR4 in hypoxia-induced signaling activation in CD49f$^+$AP$^+$GSCs, through which germ cell migration is promoted during early embryogenesis.

DISCUSSION

Niche hypoxia has been well associated with embryogenesis for organogenesis and cellular differentiation (Simon and Keith, 2008). It is highly involved in endocrine signals that regulate the symmetric self-renewal proliferation and

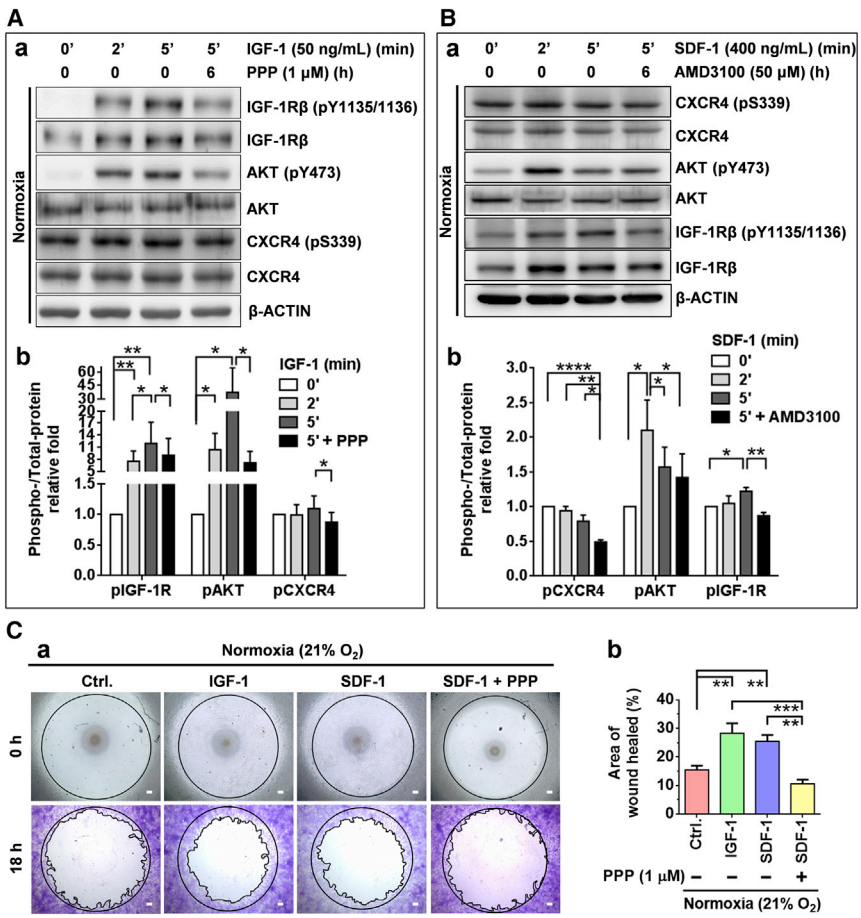

Figure 6. Crosstalk of IGF-1R and CXCR4 Signaling in Mouse CD49f$^+$AP$^+$GSCs

(A) Effect of IGF-1 (50 ng/mL), with or without PPP (1 μM) treatment, on the IGF-1R/AKT phosphorylation and CXCR4 transactivation (CXCR4 phosphorylation) of CD49f$^+$AP$^+$GSCs. (a) Western blot analysis. (b) Quantitative analysis of (a). Student's t test.

(B) Effect of SDF-1 (400 ng/mL), with or without AMD3100 (50 μM) treatment, on the CXCR4/AKT phosphorylation and IGF-1R transactivation (IGF-1R phosphorylation) of CD49f$^+$AP$^+$GSCs. (a) Western blot analysis. (b) Quantitative analysis of (a). Student's t test.

(C) Migration ability of CD49f$^+$AP$^+$GSCs with IGF-1, SDF-1, or PPP treatment for 18 hr under 21% O_2 normoxia. (a) Wound closure assay. Scale bar, 100 μm. (b) Quantitative analysis of (a). One-way ANOVA.

For all quantifications, data are the means ± SEM of at least three independent experiments. *p < 0.05, **p < 0.01, ***p < 0.001, ****p < 0.0001.

migration of embryonic GSCs (Figure 7). Two factors are strongly regulated by niche hypoxia: endocrine signals and HIFs. Hypoxia induces HIF protein expression and prevents HIF proteasomal degradation (Ginouvés et al., 2008; Haase, 2009), and HIF-2α directly induces OCT4 expression (Covello et al., 2006; Huang et al., 2014). However, whether hypoxia-mediated endocrine signaling is necessary for early embryogenesis remains largely unknown because of the lack of an appropriate *in vitro* stem cell model.

One current limitation is the lack of an *in vitro* cell model for the study of germ cell niche factors. A serum-free culture system is the most appropriate *in vitro* cell platform for monitoring the endocrine signaling of AP$^+$GSCs in response to a hypoxic environment (Huang et al., 2014). The purified CD49f$^+$AP$^+$GSCs are not fully identical to the PGCs in embryonic stage, which may raise some limitations in early germ cell studies. However, the non-cultivated CD49f$^+$AP$^+$GSCs still show similarities in the genetic and epigenetic expression profiles compared with the E11.5 PGCs and P2 AP$^+$GSCs, particularly involving pluripotency regulation in the signaling of PI3K-AKT, HIF, and chemokine proteins; thus, the serum-free CD49f$^+$AP$^+$GSC cell platform could provide the most appropriate *in vitro* cell model for exploring the role of niche hypoxia and endocrinal factors in cell proliferation and the migration of early embryonic PGC-like cells.

Symmetric division is the strategy through which embryonic germ cells enrich their stem cell number during hypoxic embryogenesis (Covello et al., 2006). Signaling induced by JAK/STAT3 or BMP controls the symmetric division of GSCs during *Drosophila* and avian development (Morrison and Kimble, 2006; Whyte et al., 2015). STAT3 is also required for mouse embryonic stem cell self-renewal proliferation and pluripotency (Niwa et al., 1998). The nucleus translocation of activated STAT3 could regulate pluripotency genes (*Oct4*, *Sox2*, and *Nanog*) (Chen et al., 2008), and constitutive STAT3 activation could regulate the expression of genes involved in premetastatic niche formation (*Sdf-1*, *Lox*, *Vegfa*, and *Mmp2*), through which microvascular tube formation and tumor metastasis are promoted (Yu et al., 2014; Psaila and Lyden, 2009) (Table S2 and Figure 2F).

Similarly, our results show that niche hypoxia not only significantly activated both IGF-1R and CXCR4 to control cell migration (Figures 3 and 5), but also activated STAT3 phosphorylation (Figures S5C and S5D), which supports

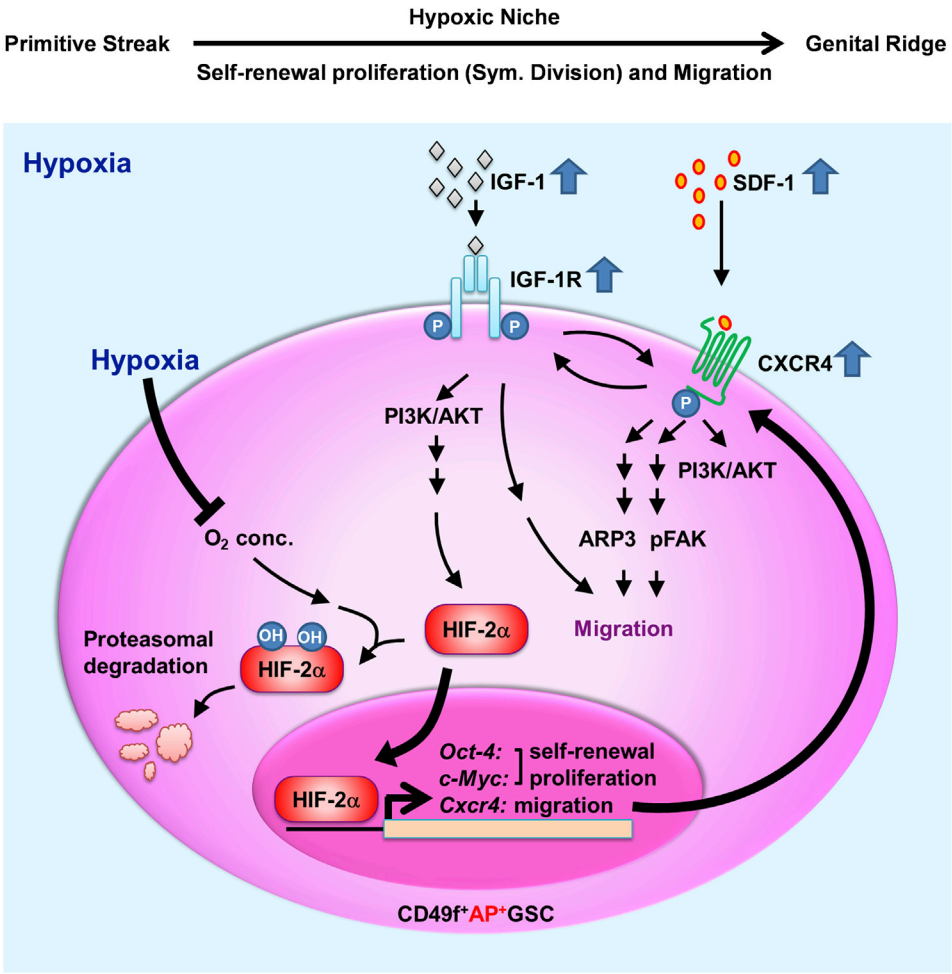

Figure 7. Proposed Working Model: IGF-1R–HIF-2α-OCT4/CXCR4 Signaling Loop Modulates Hypoxia-Derived Self-Renewal Proliferation and Migration in Mouse CD49f$^+$AP$^+$GSCs

the role of hypoxia in the self-renewal proliferation and pluripotency of embryonic stem cells (Niwa et al., 1998). STAT phosphorylation may be stimulated by the activation of numerous membrane receptors including the LIF receptor (Yu et al., 2014), IL-6 receptor (Bollrath and Greten, 2009; Chang et al., 2015; Yu et al., 2014), IGF-1R (Bollrath and Greten, 2009; Yao et al., 2016), CXCR4 (Teicher and Fricker, 2010), and VEGFR (Bollrath and Greten, 2009), etc. In support of these findings, our secretome results show high expression levels of several correspondence ligands for downstream STAT3 activation, such as SDF-1 (CXCL12, 11.6-fold) and VEGFA (5.55-fold) (Table S2; Figures 2E and 2F). Moreover, the self-renewal ability of embryonic stem cells is modulated by the IGF signaling pathway through AKT activation (Bendall et al., 2007; Huang et al., 2009).

The secretome analysis results reveal that IGFBP2, IGFBP3, IGFBP6, and IGFBP7 expression was detected in conditioned medium, highly suggesting the regulation of IGF-1R signaling under hypoxia. Consistently, hypoxia increased both IGF-1 and IGF-1Rβ expression in CD49f$^+$AP$^+$GSCs (Figures 3D and 3I). These results are further supported by the findings of recent studies that demonstrated that hypoxia increases IGF-IR expression through HIF-2α regulation (Huang et al., 2014) or through an HIF-1α/NOTCH-1/IGF-1R/AKT circuitry (Eliasz et al., 2010).

Hypoxia increases IGF-1 secretion, which directly and autocrinally activates IGF-1R phosphorylation, increases intracellular Ca^{2+} concentration, and rapidly stabilizes HIF-1α in glioma cells (Li et al., 2015). In our study, IGF-1-induced CXCR4 expression was observed to be regulated by HIF-2α (Figure 4D). The role of IGF-1R in hypoxia-induced SDF-1 and CXCR4 expression and in cell migration was demonstrated by the fact that PPP supplementation effectively suppressed hypoxia-induced cell

migration, as well as SDF-1 and CXCR4 expression in CD49f$^+$AP$^+$GSCs (Figure 5). In support, the role of IGF-1R in cell migration was further demonstrated by a recent publication, which determined an IGF-1R/STAT3/NANOG/SLUG signaling axis in stemness maintenance and epithelial-mesenchymal transition in colorectal cancer (Yao et al., 2016).

Hypoxia is important for stabilizing HIF proteins including HIF-1α and HIF-2α. In contrast to HIF-1α, the HIF-2α protein is critical for OCT4 expression because it binds to the hypoxia-response elements of the *Oct4* promoter region to initiate OCT4 expression in cells under O_2 deprivation (hypoxia) conditions (Covello et al., 2006; Hu et al., 2003). Knockout of HIF-2α dramatically reduces the PGC number in the genital ridge, strongly highlighting the critical role of OCT4 in embryonic PGC survival (Covello et al., 2006). HIF-2α nucleus translocation also plays a critical role in the transcriptional activation of *Cxcr4 in* clear cell renal carcinomas (Staller et al., 2003) and *c-Myc* in cancer cells (Gordan et al., 2007). Together, these data strongly suggest the central role of HIF-2α in cell self-renewal proliferation (OCT4 and c-Myc) and migration (CXCR4) under embryonic hypoxia.

Hypoxia is a major inducer of endocrine factors, such as VEGF, through HIF-2α regulation in embryogenesis (Covello et al., 2006). VEGF was discovered to maintain cell survival autocrinally (Domigan et al., 2015), enhance sphere formation, and regulate the self-renewal of liver cancer stem cells (Kwon et al., 2016). In early AP$^+$GSCs, VEGFA was significantly upregulated by up to 5.55-fold. This observation highlights the potential role of VEGFA in AP$^+$GSC survival under embryonic hypoxia (Table S2).

Previous studies have reported that MMP2 reduction can lead to the differentiation of human mesenchymal stem cells (Cronwright et al., 2005), suggesting the role of MMP2 in stemness maintenance. In our study, we found that hypoxia increased the MMP2 expression level in AP$^+$GSCs by up to 5.02-fold (Table S2), supporting the effect of hypoxia on the stemness maintenance and proliferation of AP$^+$GSCs (Huang et al., 2014). THBS2 and VCAN are localized in the extracellular matrix to regulate cell adhesion as well as collagen remodeling, which is essential for cancer progression and metastasis (Cheon et al., 2014). THBS2 has been demonstrated to mediate the adhesion of human hematopoietic stem/progenitor cells (Muth et al., 2013) and is associated with cell growth and embryogenesis (Laherty et al., 1992). VCAN has been reported to increase the spheroid formation in prostate cancer cells (Oktem et al., 2014). Importantly, hypoxia highly upregulated SDF-1 expression in AP$^+$GSCs (Figure 3 and Table S2). SDF1/CXCR4 signaling is essential for the self-renewal of SSCs (Chen and Liu, 2015; Yang et al., 2013). In the present study, the cooperative network of secretion proteins, including SDF-1, VEGFA, MMP2, THBS2, and VCAN, was upregulated under the hypoxic condition (Table S2 and Figure 2F, red line). These results highlight the synergistic cooperation of hypoxia-induced gene expression levels, at least in part, in the self-renewal and migration of AP$^+$GSCs.

Taken together, in the current study, we used primary CD49f$^+$AP$^+$GSCs and a serum-free culture system to demonstrate that niche hypoxia promotes the symmetric self-renewal proliferation (Huang et al., 2014) and migration of embryonic CD49f$^+$AP$^+$GSCs through the hypoxia-induced IGF-1R–HIF-2α-OCT4/CXCR4 signaling loop (Figure 7). IGF-1 activates IGF-1Rβ (pY1135/1136)/PI3K/AKT (pY473), after which it coordinates with the hypoxic effects to increase HIF-2α protein levels. HIF-2α translocates into the nucleus to initiate the transcriptional activation of *Oct4*, *c-Myc*, and *Cxcr4*, through which the symmetric self-renewal proliferation (*Oct4* and *c-Myc*) and cell migration (*Cxcr4*) are maintained. CXCR4 responds to hypoxia-induced SDF-1 to activate CXCR4 phosphorylation (pS339). SDF-1/CXCR4 activation would induce FAK phosphorylation and ARP3 membrane translocation, which drive the migration ability of early GSCs. Meanwhile, crosstalk was observed between the activated p-IGF-1Rβ and p-CXCR4. In summary, we demonstrate that niche hypoxia promotes the IGF-1R/HIF-2α/CXCR4 signaling loop to initiate symmetric proliferation and cell migration in early CD49f$^+$AP$^+$GSCs (Figure 7). The findings of our studies provide critical insights into how niche hypoxia cooperates with its associated endocrine signals to regulate both self-renewal symmetric division and migration during early germ cell development.

EXPERIMENTAL PROCEDURES

Cultivation of Mouse AP$^+$GSCs in Serum-free Culture Medium

ICR mice were obtained from the National Laboratory Animal Center and National Applied Research Laboratories (Taipei, Taiwan). The animal study protocol was approved by the Institutional Animal Care and Use Committee or Panel (IACUC/IACUP) at Taipei Medical University (Affidavit of Approval of Animal Use Protocol # LAC-2016-0108). Mouse AP$^+$GSCs were generated as previously described (Huang et al., 2009). In brief, the gonads of E11.5 embryos and testes of 0- to 2-day-old postpartum newborn ICR mice were collected and briefly washed in Hank's buffer (Gibco BRL, Grand Island, NY, USA) before treatment with 0.1% protease type-XIV (Sigma-Aldrich, St. Louis, MO, USA) in MCDB-201 medium (Sigma-Aldrich) at 4°C for 16–20 hr. In general, one digested testis could yield approximately 1.5 × 10^5 cells. For formation of PGC and AP$^+$GSC colonies, total gonadal or testicular cells were resuspended in MCDB-201 medium supplemented with 1× insulin, transferrin, and selenium, and 10 ng/mL epidermal growth factor (Gibco BRL). The gonadal or testicular cells were seeded on a

laminin-coated culture plate (200 ng/cm^2, Sigma-Aldrich) at a density of 8 × 10^4 cells/cm^2 and cultivated for 7 days at 37°C under a 21%, 5%, 3%, or 1% O_2 atmosphere.

Purification of CD49f$^+$ Mouse GSCs

CD49f$^+$GSCs were purified using a MACS (Miltenyi Biotec, Bergisch Gladbach, Germany), as described previously (Huang et al., 2014). In brief, the total testicular cells were incubated with phycoerythrin (PE)-conjugated antibody against CD49f (eBioscience, San Diego, CA, USA) for 1 hr on ice. CD49f-labeled cells were washed and then incubated with anti-PE microbeads (Miltenyi Biotec) for 40 min at 4°C. Stained cells were separated using a MACS column (Miltenyi Biotec) according to the manufacturer's recommended protocol. The purified CD49f$^+$ cells were directly used in transcriptomic and epigenetic analyses. For other experiments, the purified CD49f$^+$ cells were then cultivated on a laminin-coated culture plate (400 ng/cm^2).

Statistical Analysis

All experiments were repeated at least three times with individual samples. The results are presented as the mean ± SD or median (SEM), as appropriate. Differences in means were assessed using a t test, one-way ANOVA, or two-way ANOVA (GraphPad InStat 6.0, GraphPad Software, La Jolla, CA, USA). A p value of < 0.05 was considered statistically significant.

ACCESSION NUMBERS

Microarray data for each gene are available in the GEO database under accession number GEO: GSE106664.

SUPPLEMENTAL INFORMATION

Supplemental Information includes Supplemental Experimental Procedures, seven figures, and four tables and can be found with this article online at https://doi.org/10.1016/j.stemcr.2017.12.003.

AUTHOR CONTRIBUTIONS

Conception and Design, Y.-C.K., H.-K.A., and Y.-H.H. Administrative, Technical, or Material Support, Y.-C.K., J.-L.H., Y.-C.W., S.-W.P., and Y.-H.H. Development of Methodology, Y.-C.K. and Y.-C.W. Acquisition of Data, Y.-C.K., J.-L.H., H.-F.W., C.-J.L., S.-W.P., and S.-C.L. Analysis and Interpretation of Data, Y.-C.K., H.-K.A., Y.-C.W., and Y.-H.H. Writing, Review, and/or Revision of the Manuscript, Y.-C.K., H.-K.A., H.-N.H., and Y.-H.H. Study Supervision, Y.-H.H.

ACKNOWLEDGMENTS

This work was financially supported by research grants from the National Science Council, Taiwan (NSC102-2628-B-038-008-MY3); the Ministry of Science and Technology, Taiwan (MOST 103-2321-B-038-011, MOST 104-2321-B-038-003, MOST 105-2628-B-038-008-MY3, MOST 106-2314-B-038-074, and MOST 106-3114-B-038-001); the Health and Welfare Surcharge of Tobacco Products (MOHW105-TDU-B-212-134001 and MOHW106-TDU-B-212-144001); Taipei Medical University (TMU-T104-06, TMU-T105-06, TMU-T106-03, 105TMU-CIT-01-3, and 106TMU-CIT-01-3); and Taipei Medical University Hospital (103TMU-TMUH-05, 104TMU-TMUH-04, and 105TMU-TMUH-10).

Received: April 4, 2017
Revised: December 1, 2017
Accepted: December 5, 2017
Published: January 4, 2018

REFERENCES

Anderson, R., Fassler, R., Georges-Labouesse, E., Hynes, R.O., Bader, B.L., Kreidberg, J.A., Schaible, K., Heasman, J., and Wylie, C. (1999). Mouse primordial germ cells lacking beta1 integrins enter the germline but fail to migrate normally to the gonads. Development *126*, 1655–1664.

Barnes, D., and Sato, G. (1980). Serum-free cell culture: a unifying approach. Cell *22*, 649–655.

Barriga, E.H., Maxwell, P.H., Reyes, A.E., and Mayor, R. (2013). The hypoxia factor Hif-1α controls neural crest chemotaxis and epithelial to mesenchymal transition. J. Cell Biol. *201*, 759–776.

Bendall, S.C., Stewart, M.H., Menendez, P., George, D., Vijayaragavan, K., Werbowetski-Ogilvie, T., Ramos-Mejia, V., Rouleau, A., Yang, J., Bossé, M., et al. (2007). IGF and FGF cooperatively establish the regulatory stem cell niche of pluripotent human cells in vitro. Nature *448*, 1015–1021.

Bollrath, J., and Greten, F.R. (2009). IKK/NF-kappaB and STAT3 pathways: central signalling hubs in inflammation-mediated tumour promotion and metastasis. EMBO Rep. *10*, 1314–1319.

Brinster, R.L. (2002). Germline stem cell transplantation and transgenesis. Science *296*, 2174–2176.

Chang, T.S., Wu, Y.C., Chi, C.C., Su, W.C., Chang, P.J., Lee, K.F., Tung, T.H., Wang, J., Liu, J.J., Tung, S.Y., et al. (2015). Activation of IL6/IGFIR confers poor prognosis of HBV-related hepatocellular carcinoma through induction of OCT4/NANOG expression. Clin. Cancer Res. *21*, 201–210.

Chen, S.R., and Liu, Y.X. (2015). Regulation of spermatogonial stem cell self-renewal and spermatocyte meiosis by Sertoli cell signaling. Reproduction *149*, R159–R167.

Chen, X., Xu, H., Yuan, P., Fang, F., Huss, M., Vega, V.B., Wong, E., Orlov, Y.L., Zhang, W., Jiang, J., et al. (2008). Integration of external signaling pathways with the core transcriptional network in embryonic stem cells. Cell *133*, 1106–1117.

Cheon, D.J., Tong, Y., Sim, M.S., Dering, J., Berel, D., Cui, X., Lester, J., Beach, J.A., Tighiouart, M., Walts, A.E., et al. (2014). A collagen-remodeling gene signature regulated by TGF-beta signaling is associated with metastasis and poor survival in serous ovarian cancer. Clin. Cancer Res. *20*, 711–723.

Chuva de Sousa Lopes, S.M., van den Driesche, S., Carvalho, R.L., Larsson, J., Eggen, B., Surani, M.A., and Mummery, C.L. (2005). Altered primordial germ cell migration in the absence of transforming growth factor beta signaling via ALK5. Dev. Biol. *284*, 194–203.

Covello, K.L., Kehler, J., Yu, H., Gordan, J.D., Arsham, A.M., Hu, C.J., Labosky, P.A., Simon, M.C., and Keith, B. (2006). HIF-2alpha

regulates Oct-4: effects of hypoxia on stem cell function, embryonic development, and tumor growth. Genes Dev. *20*, 557–570.

Cronwright, G., Le Blanc, K., Gotherstrom, C., Darcy, P., Ehnman, M., and Brodin, B. (2005). Cancer/testis antigen expression in human mesenchymal stem cells: down-regulation of SSX impairs cell migration and matrix metalloproteinase 2 expression. Cancer Res. *65*, 2207–2215.

Dang, I., Gorelik, R., Sousa-Blin, C., Derivery, E., Guérin, C., Linkner, J., Nemethova, M., Dumortier, J.G., Giger, F.A., Chipysheva, T.A., et al. (2013). Inhibitory signalling to the Arp2/3 complex steers cell migration. Nature *503*, 281–284.

DeMali, K.A., and Burridge, K. (2003). Coupling membrane protrusion and cell adhesion. J. Cell Sci. *116*, 2389–2397.

Doitsidou, M., Reichman-Fried, M., Stebler, J., Koprunner, M., Dorries, J., Meyer, D., Esguerra, C.V., Leung, T., and Raz, E. (2002). Guidance of primordial germ cell migration by the chemokine SDF-1. Cell *111*, 647–659.

Domigan, C.K., Warren, C.M., Antanesian, V., Happel, K., Ziyad, S., Lee, S., Krall, A., Duan, L., Torres-Collado, A.X., Castellani, L.W., et al. (2015). Autocrine VEGF maintains endothelial survival through regulation of metabolism and autophagy. J. Cell Sci. *128*, 2236–2248.

Eliasz, S., Liang, S., Chen, Y., De Marco, M.A., Machek, O., Skucha, S., Miele, L., and Bocchetta, M. (2010). Notch-1 stimulates survival of lung adenocarcinoma cells during hypoxia by activating the IGF-1R pathway. Oncogene *29*, 2488–2498.

Fischer, B., and Bavister, B.D. (1993). Oxygen tension in the oviduct and uterus of rhesus monkeys, hamsters and rabbits. J. Reprod. Fertil. *99*, 673–679.

Forristal, C.E., Wright, K.L., Hanley, N.A., Oreffo, R.O., and Houghton, F.D. (2010). Hypoxia inducible factors regulate pluripotency and proliferation in human embryonic stem cells cultured at reduced oxygen tensions. Reproduction *139*, 85–97.

Free, M.J., Schluntz, G.A., and Jaffe, R.A. (1976). Respiratory gas tensions in tissues and fluids of the male rat reproductive tract. Biol. Reprod. *14*, 481–488.

Ginouvés, A., Ilc, K., Macias, N., Pouysségur, J., and Berra, E. (2008). PHDs overactivation during chronic hypoxia "desensitizes" HIFalpha and protects cells from necrosis. Proc. Natl. Acad. Sci. USA *105*, 4745–4750.

Ginsburg, M., Snow, M.H., and McLaren, A. (1990). Primordial germ cells in the mouse embryo during gastrulation. Development *110*, 521–528.

Gordan, J.D., Bertout, J.A., Hu, C.J., Diehl, J.A., and Simon, M.C. (2007). HIF-2alpha promotes hypoxic cell proliferation by enhancing c-myc transcriptional activity. Cancer Cell *11*, 335–347.

Haase, V.H. (2009). The VHL tumor suppressor: master regulator of HIF. Curr. Pharm. Des. *15*, 3895–3903.

Hartwig, J., Tarbashevich, K., Seggewiß, J., Stehling, M., Bandemer, J., Grimaldi, C., Paksa, A., Groß-Thebing, T., Meyen, D., and Raz, E. (2014). Temporal control over the initiation of cell motility by a regulator of G-protein signaling. Proc. Natl. Acad. Sci. USA *111*, 11389–11394.

Ho, L., Tan, S.Y., Wee, S., Wu, Y., Tan, S.J., Ramakrishna, N.B., Chng, S.C., Nama, S., Szczerbinska, I., Chan, Y.S., et al. (2015). ELABELA is an endogenous growth factor that sustains hESC self-renewal via the PI3K/AKT pathway. Cell Stem Cell *17*, 435–447.

Hoei-Hansen, C.E., Sehested, A., Juhler, M., Lau, Y.F., Skakkebaek, N.E., Laursen, H., and Rajpert-de Meyts, E. (2006). New evidence for the origin of intracranial germ cell tumours from primordial germ cells: expression of pluripotency and cell differentiation markers. J. Pathol. *209*, 25–33.

Hu, C.J., Wang, L.Y., Chodosh, L.A., Keith, B., and Simon, M.C. (2003). Differential roles of hypoxia-inducible factor 1alpha (HIF-1alpha) and HIF-2alpha in hypoxic gene regulation. Mol. Cell. Biol. *23*, 9361–9374.

Huang, Y.H., Chin, C.C., Ho, H.N., Chou, C.K., Shen, C.N., Kuo, H.C., Wu, T.J., Wu, Y.C., Hung, Y.C., Chang, C.C., et al. (2009). Pluripotency of mouse spermatogonial stem cells maintained by IGF-1- dependent pathway. FASEB J. *23*, 2076–2087.

Huang, Y.H., Lin, M.H., Wang, P.C., Wu, Y.C., Chiang, H.L., Wang, Y.L., Chang, J.H., Huang, Y.K., Gu, S.Y., Ho, H.N., et al. (2014). Hypoxia inducible factor 2α/insulin-like growth factor receptor signal loop supports the proliferation and Oct-4 maintenance of mouse germline stem cells. Mol. Hum. Reprod. *20*, 526–537.

Kwon, T., Bak, Y., Park, Y.H., Jang, G.B., Nam, J.S., Yoo, J.E., Park, Y.N., Bak, I.S., Kim, J.M., Yoon, D.Y., et al. (2016). Peroxiredoxin II is essential for maintaining stemness by redox regulation in liver cancer cells. Stem Cells *34*, 1188–1197.

Laherty, C.D., O'Rourke, K., Wolf, F.W., Katz, R., Seldin, M.F., and Dixit, V.M. (1992). Characterization of mouse thrombospondin 2 sequence and expression during cell growth and development. J. Biol. Chem. *267*, 3274–3281.

Lawson, K.A., Dunn, N.R., Roelen, B.A., Zeinstra, L.M., Davis, A.M., Wright, C.V., Korving, J.P., and Hogan, B.L. (1999). Bmp4 is required for the generation of primordial germ cells in the mouse embryo. Genes Dev. *13*, 424–436.

Le Clainche, C., and Carlier, M.F. (2008). Regulation of actin assembly associated with protrusion and adhesion in cell migration. Physiol. Rev. *88*, 489–513.

Li, S., Wang, J., Wei, Y., Liu, Y., Ding, X., Dong, B., Xu, Y., and Wang, Y. (2015). Crucial role of TRPC6 in maintaining the stability of HIF-1α in glioma cells under hypoxia. J. Cell Sci. *128*, 3317–3329.

McLaren, A. (2003). Primordial germ cells in the mouse. Dev. Biol. *262*, 1–15.

Molyneaux, K.A., Zinszner, H., Kunwar, P.S., Schaible, K., Stebler, J., Sunshine, M.J., O'Brien, W., Raz, E., Littman, D., Wylie, C., et al. (2003). The chemokine SDF1/CXCL12 and its receptor CXCR4 regulate mouse germ cell migration and survival. Development *130*, 4279–4286.

Morrison, S.J., and Kimble, J. (2006). Asymmetric and symmetric stem-cell divisions in development and cancer. Nature *441*, 1068–1074.

Muth, C.A., Steinl, C., Klein, G., and Lee-Thedieck, C. (2013). Regulation of hematopoietic stem cell behavior by the nanostructured presentation of extracellular matrix components. PLoS One *8*, e54778.

Niwa, H., Burdon, T., Chambers, I., and Smith, A. (1998). Self-renewal of pluripotent embryonic stem cells is mediated via activation of STAT3. Genes Dev. *12*, 2048–2060.

Ohinata, Y., Payer, B., O'Carroll, D., Ancelin, K., Ono, Y., Sano, M., Barton, S.C., Obukhanych, T., Nussenzweig, M., Tarakhovsky, A., et al. (2005). Blimp1 is a critical determinant of the germ cell lineage in mice. Nature *436*, 207–213.

Oktem, G., Sercan, O., Guven, U., Uslu, R., Uysal, A., Goksel, G., Ayla, S., and Bilir, A. (2014). Cancer stem cell differentiation: TGFbeta1 and versican may trigger molecules for the organization of tumor spheroids. Oncol. Rep. *32*, 641–649.

Psaila, B., and Lyden, D. (2009). The metastatic niche: adapting the foreign soil. Nat. Rev. Cancer *9*, 285–293.

Raz, E. (2004). Guidance of primordial germ cell migration. Curr. Opin. Cell Biol. *16*, 169–173.

Saga, Y. (2008). Mouse germ cell development during embryogenesis. Curr. Opin. Genet. Dev. *18*, 337–341.

Saitou, M., Barton, S.C., and Surani, M.A. (2002). A molecular programme for the specification of germ cell fate in mice. Nature *418*, 293–300.

Scortegagna, M., Ding, K., Oktay, Y., Gaur, A., Thurmond, F., Yan, L.J., Marck, B.T., Matsumoto, A.M., Shelton, J.M., Richardson, J.A., et al. (2003). Multiple organ pathology, metabolic abnormalities and impaired homeostasis of reactive oxygen species in Epas1–/– mice. Nat. Genet. *35*, 331–340.

Simon, M.C., and Keith, B. (2008). The role of oxygen availability in embryonic development and stem cell function. Nat. Rev. Mol. Cell Biol. *9*, 285–296.

Staller, P., Sulitkova, J., Lisztwan, J., Moch, H., Oakeley, E.J., and Krek, W. (2003). Chemokine receptor CXCR4 downregulated by von Hippel-Lindau tumour suppressor pVHL. Nature *425*, 307–311.

Sugiyama, T., Kohara, H., Noda, M., and Nagasawa, T. (2006). Maintenance of the hematopoietic stem cell pool by CXCL12-CXCR4 chemokine signaling in bone marrow stromal cell niches. Immunity *25*, 977–988.

Teicher, B.A., and Fricker, S.P. (2010). CXCL12 (SDF-1)/CXCR4 pathway in cancer. Clin. Cancer Res. *16*, 2927–2931.

Tu, T.C., Nagano, M., Yamashita, T., Hamada, H., Ohneda, K., Kimura, K., and Ohneda, O. (2016). A chemokine receptor, CXCR4, which is regulated by hypoxia-inducible factor 2α, is crucial for functional endothelial progenitor cells migration to ischemic tissue and wound repair. Stem Cells Dev. *25*, 266–276.

Turner, C.E. (2000). Paxillin and focal adhesion signalling. Nat. Cell Biol. *2*, E231–E236.

Whyte, J., Glover, J.D., Woodcock, M., Brzeszczynska, J., Taylor, L., Sherman, A., Kaiser, P., and McGrew, M.J. (2015). FGF, insulin, and SMAD signaling cooperate for avian primordial germ cell self-renewal. Stem Cell Reports *5*, 1171–1182.

Yang, Q.E., Kim, D., Kaucher, A., Oatley, M.J., and Oatley, J.M. (2013). CXCL12-CXCR4 signaling is required for the maintenance of mouse spermatogonial stem cells. J. Cell Sci. *126*, 1009–1020.

Yao, C., Su, L., Shan, J., Zhu, C., Liu, L., Liu, C., Xu, Y., Yang, Z., Bian, X., Shao, J., et al. (2016). IGF/STAT3/NANOG/slug signaling axis simultaneously controls epithelial-mesenchymal transition and stemness maintenance in colorectal cancer. Stem Cells *34*, 820–831.

Ying, Y., Qi, X., and Zhao, G.Q. (2001). Induction of primordial germ cells from murine epiblasts by synergistic action of BMP4 and BMP8B signaling pathways. Proc. Natl. Acad. Sci. USA *98*, 7858–7862.

Yu, H., Lee, H., Herrmann, A., Buettner, R., and Jove, R. (2014). Revisiting STAT3 signalling in cancer: new and unexpected biological functions. Nat. Rev. Cancer *14*, 736–746.

Stem Cell Reports, Volume *10*

Supplemental Information

IGF-1R Promotes Symmetric Self-Renewal and Migration of Alkaline Phosphatase^{+} Germ Stem Cells through HIF-2α-OCT4/CXCR4 Loop under Hypoxia

Yung-Che Kuo, Heng-Kien Au, Jue-Liang Hsu, Hsiao-Feng Wang, Chiung-Ju Lee, Syue-Wei Peng, Ssu-Chuan Lai, Yu-Chih Wu, Hong-Nerng Ho, and Yen-Hua Huang

Supplemental information

Supplemental Figures:

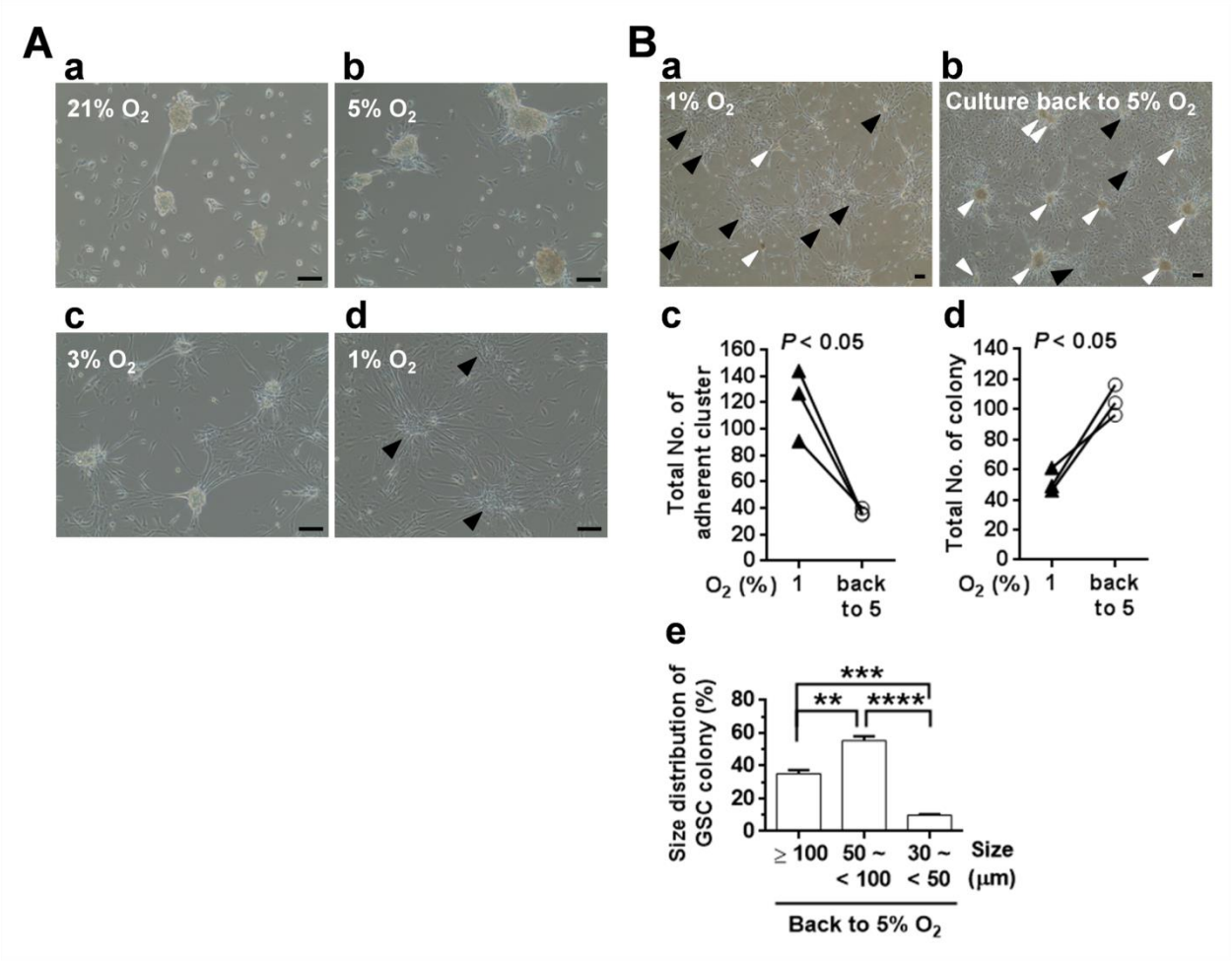

Figure S1. Effect of oxygen tension on AP$^+$GSC colony formation under a serum-free culture condition. (Related to main Figure 2.)

A. (a-c) Colony morphology of mouse P2 AP$^+$GSCs under normoxia (21% O_2) and hypoxia (5% and 3% O_2). **(d)** Cluster of mesenchymal-like cells under 1% O_2 hypoxia (black arrowhead). Scale bar, 100 μm. **B.** GSC colony re-formation assay. **(a)** The P2 AP$^+$GSCs were cultivated under hypoxia (1% O_2) for 7 days and **(b)** re-placed in 5% O_2 for another 7 days. Black arrowhead, GSC adherent cluster; white arrowhead, GSC colony. Scale bar, 100 μm. **(c)** Quantification of the GSC adherent cluster number, **(d)** colony number, and **(e)** colony size distribution. Data are mean ± SEM of at least three independent experiments. *P < 0.05, **P < 0.01, ***P < 0.001, ****P < 0.0001. Student's t test **(c and d)** and one-way ANOVA **(e)**.

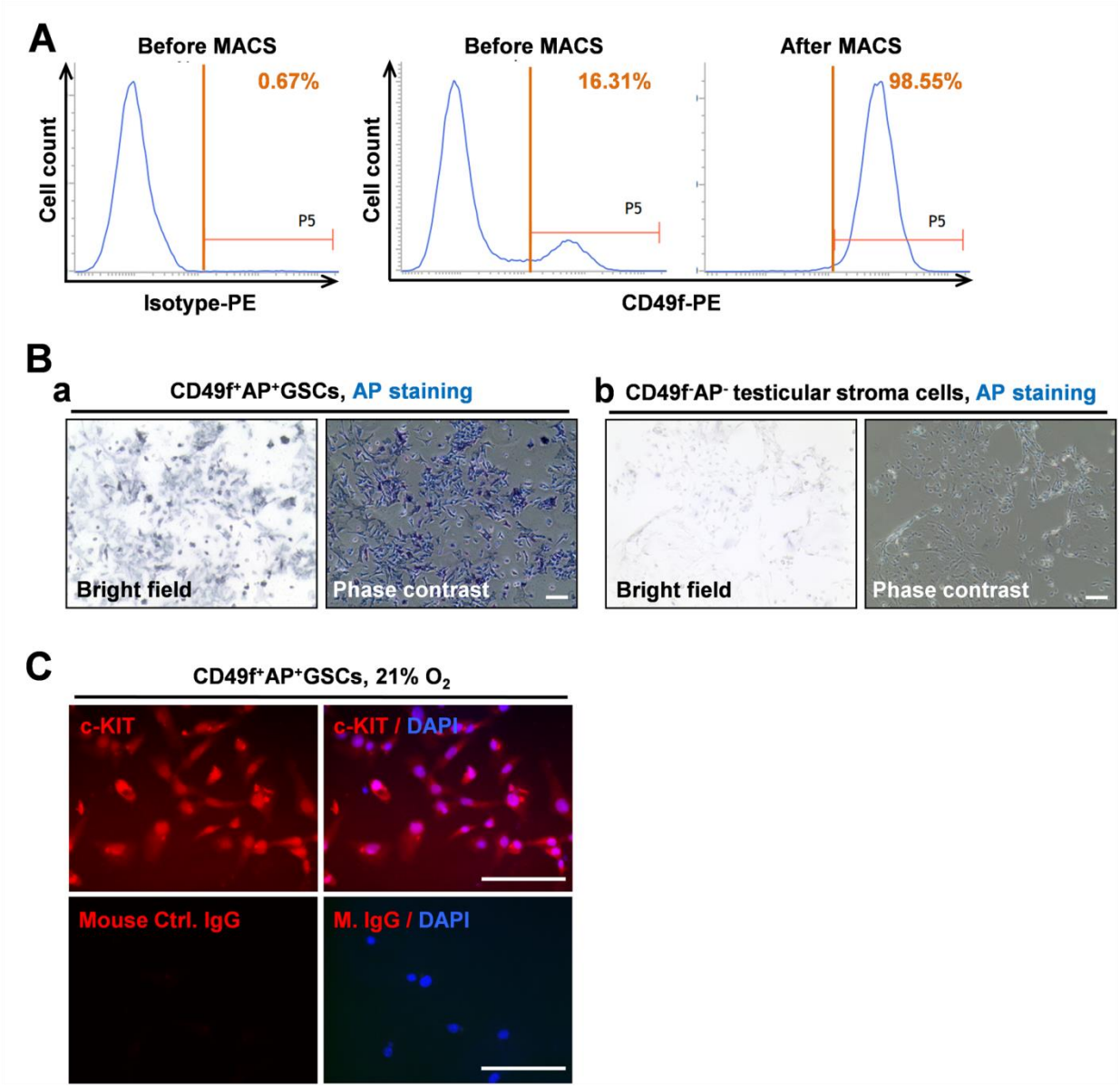

Figure S2. MACS isolation and characterization of CD49f$^+$AP$^+$GSCs. (Related to main Figure 3.)

A. Purification of CD49f$^+$AP$^+$GSCs using an MACS. The purity of the CD49f$^+$ cell population (P5 region) was analyzed using flow cytometry. **B.** Alkaline phosphatase staining (in blue) of **(a)** CD49f$^+$AP$^+$GSCs and **(b)** CD49f$^-$AP$^-$testicular cells cultivated under 5% O_2 hypoxia. Scale bar, 100 μm. **C.** Immunofluorescence staining of germ cell-specific proteins in CD49f$^+$AP$^+$GSCs under normoxia. Scale bar, 100 μm.

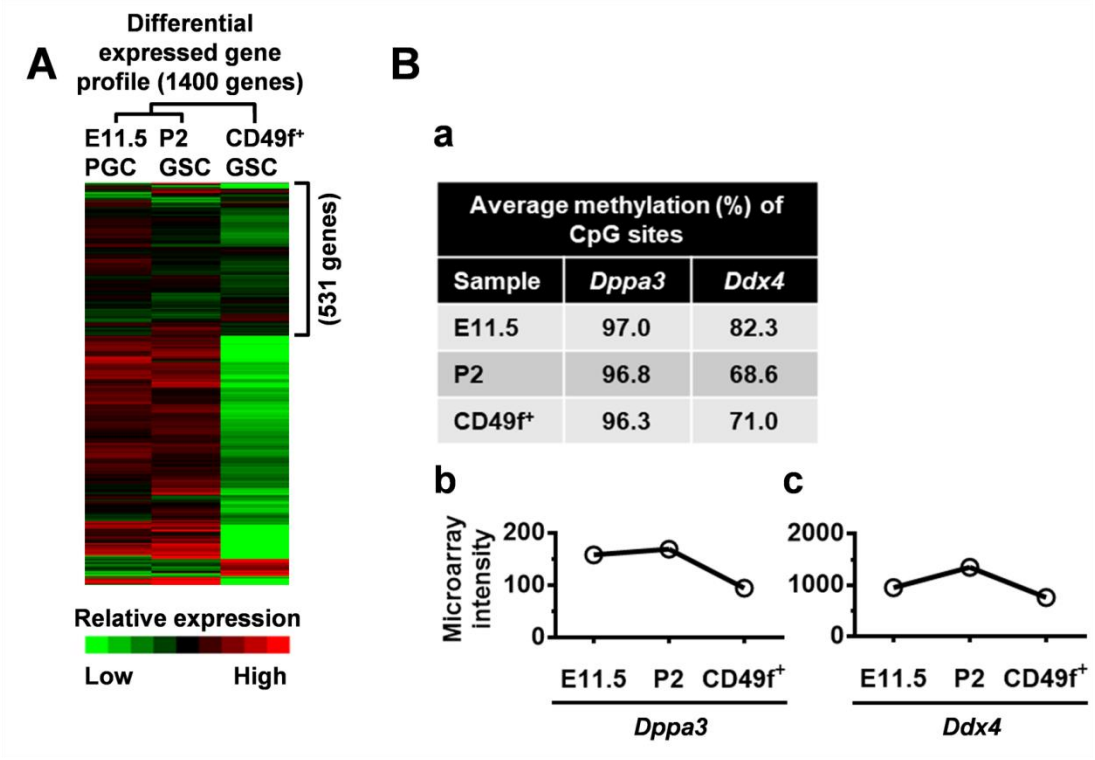

Figure S3. Transcriptome and epigenetic expression patterns of E11.5 PGCs, P2 AP$^+$GSCs, and CD49f$^+$AP$^+$GSCs. (Related to main Figures 1 and 3.)

A. Heatmap of global gene expression pattern of E11.5 PGCs, P2 AP$^+$GSCs, and purified AP$^+$CD49f$^+$GSCs. **B.** Epigenetic and gene expression analysis of *Dppa3* and *Ddx4*. **(a)** Bisulfite genomic sequencing. **(b and c)** Gene expression levels from a microarray analysis.

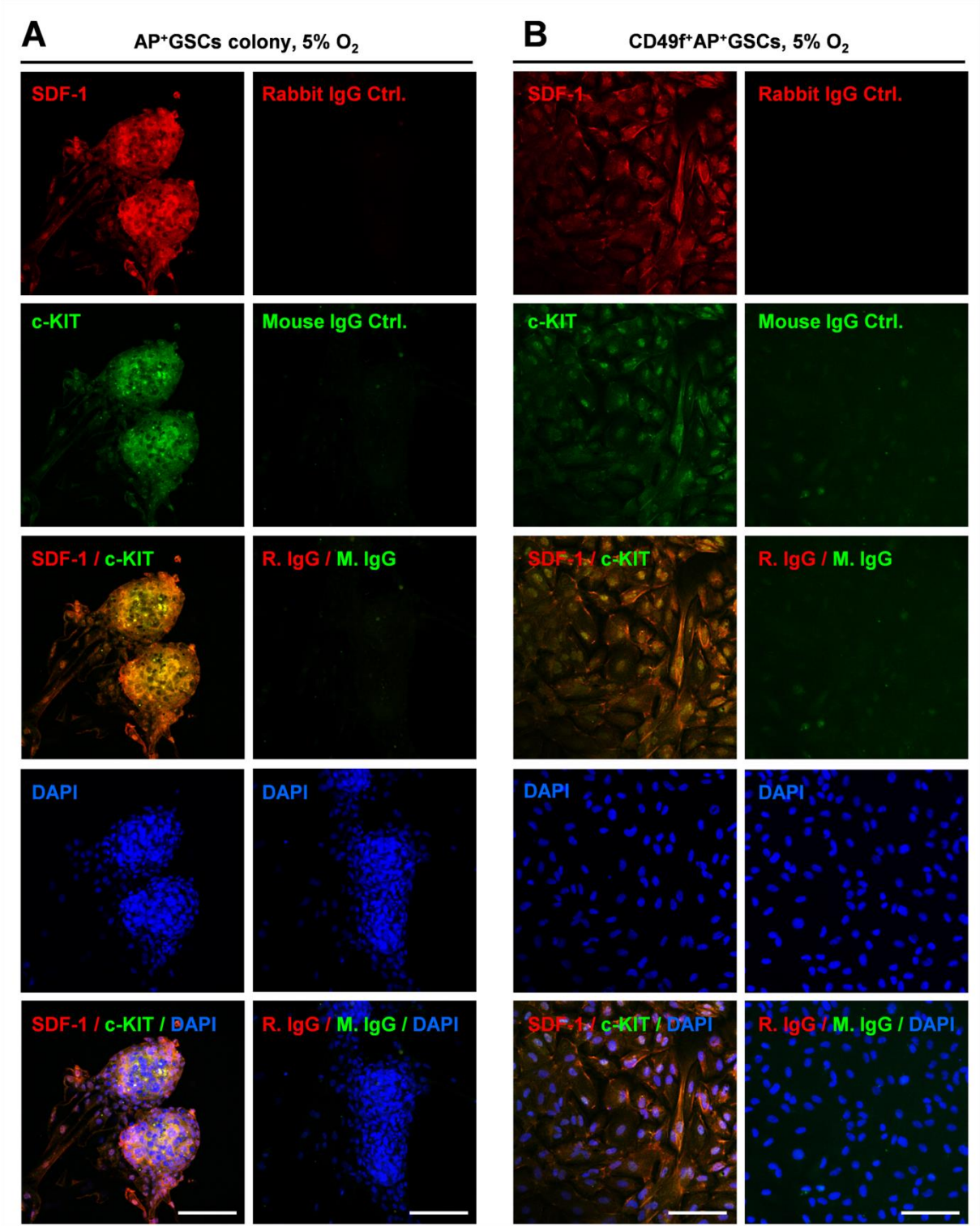

Figure S4. Immunostaining of SDF-1 and c-KIT in AP$^+$GSC colonies and CD49f$^+$AP$^+$GSCs. (Related to main Figure 3.)

Immunofluorescence staining of SDF-1 and c-KIT in **(A)** AP$^+$GSC colonies and **(B)** CD49f$^+$AP$^+$GSCs under 5% O_2 hypoxia. Negative immunostaining controls (IgG) are shown. Scale bar, 100 μm.

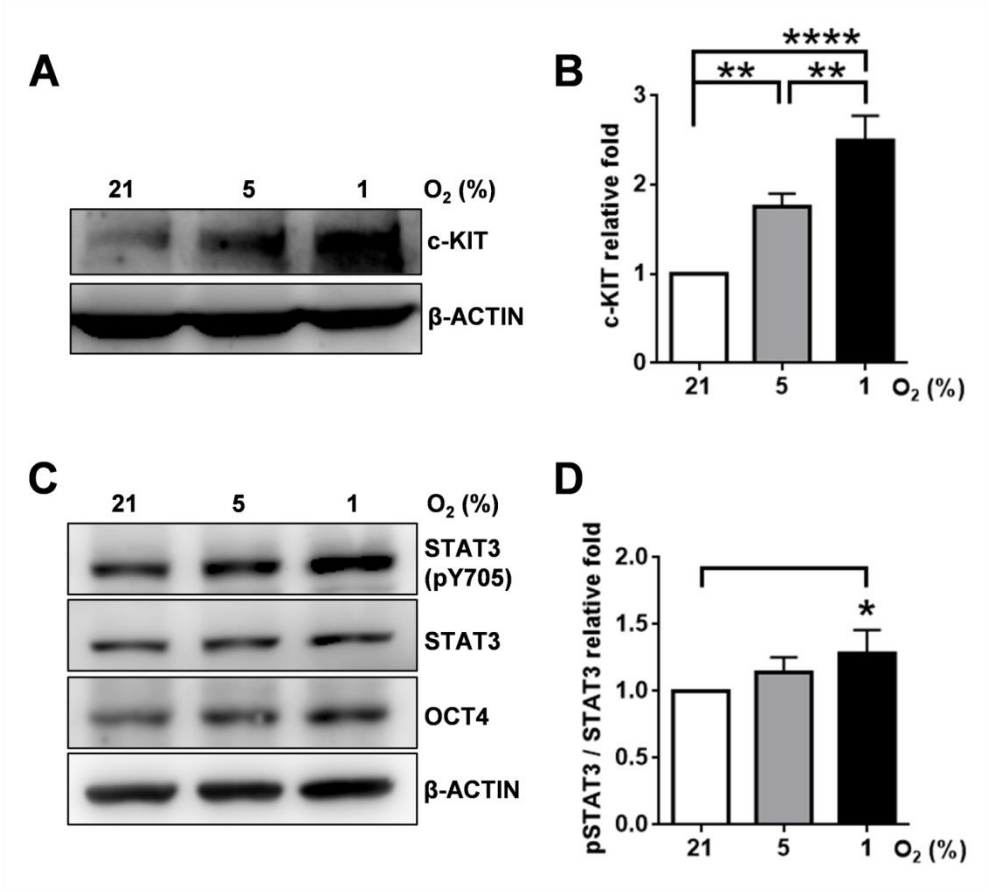

Figure S5. Effect of hypoxia on c-KIT, phospho-STAT3, and OCT4 expression in CD49f$^+$AP$^+$GSCs. (Related to main Figures 2 and 3.)

A. Effect of different oxygen tension (21%, 5%, and 1% O_2 for 24 h) on c-KIT expression levels of CD49f$^+$AP$^+$GSCs (Western blot analysis). **B.** Quantitative analysis of **(A)**. Data are the means ± SEM of at least three independent experiments. One-way ANOVA. $^{**}P < 0.01$, $^{****}P < 0.0001$. **C.** Cells were cultivated under different oxygen tension of 21%, 5%, and 1% O_2 for 24 h. The protein levels of STAT3, phospho-STAT3 (pY705), and OCT4 of CD49f$^+$AP$^+$GSCs are shown. Western blot analysis. **D.** Quantitative analysis of **(C)**. Data are the means ± SEM of at least three independent experiments. One-way ANOVA. $^{*}P < 0.05$.

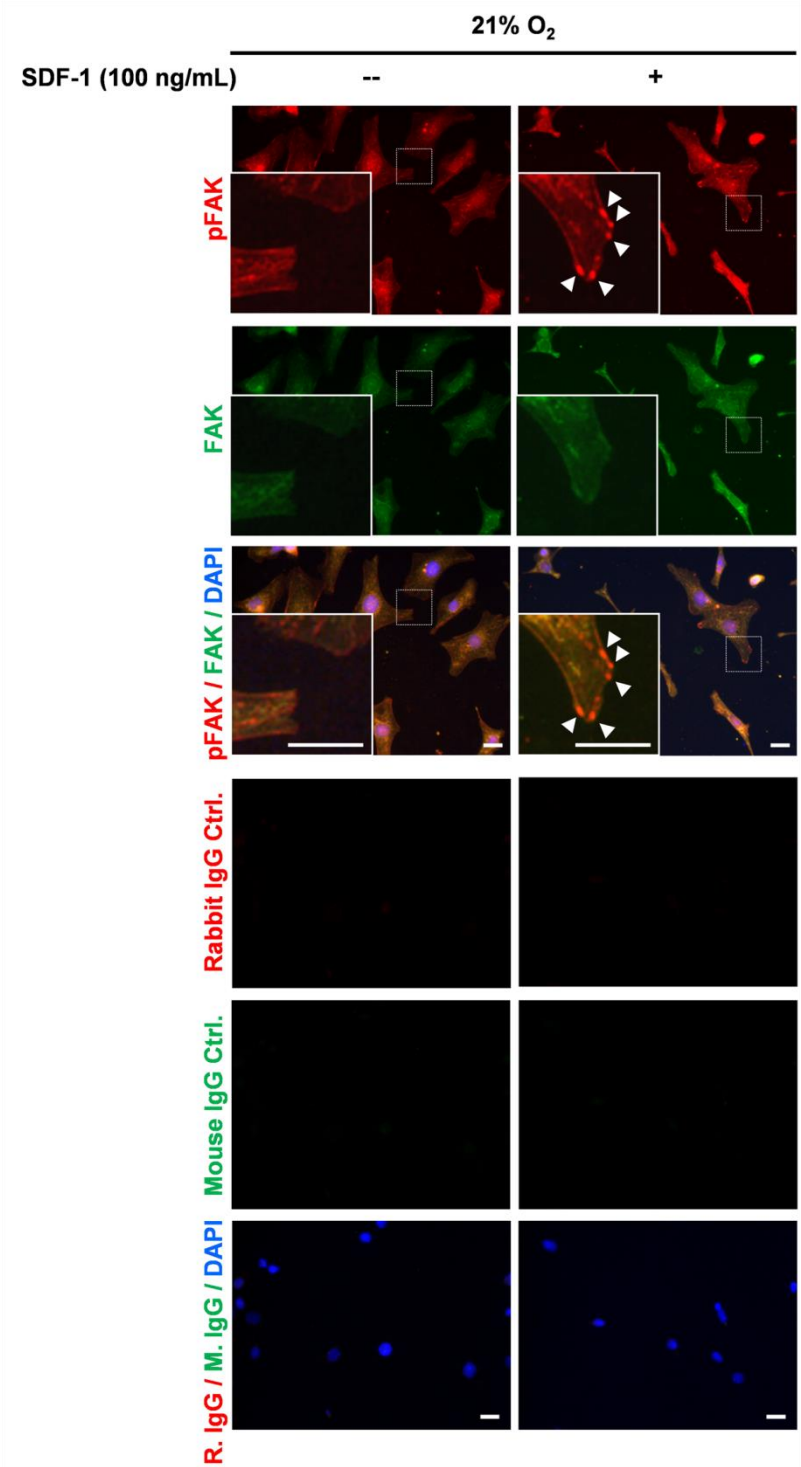

Figure S6. Effect of SDF-1 on phospho-FAK levels in CD49f^{+}AP^{+}GSCs under normoxia. (Related to main Figure 3.) The CD49f^{+}AP^{+}GSCs were treated with or without SDF-1 (100 ng/mL) for 48 h under normoxia (21% O_2). The levels of pFAK and FAK were detected by immunofluorescence staining. Negative immunostaining controls (IgG) are shown. Arrowheads indicate the specific cellular protein localization of pFAK. Scale bar, 20 μm.

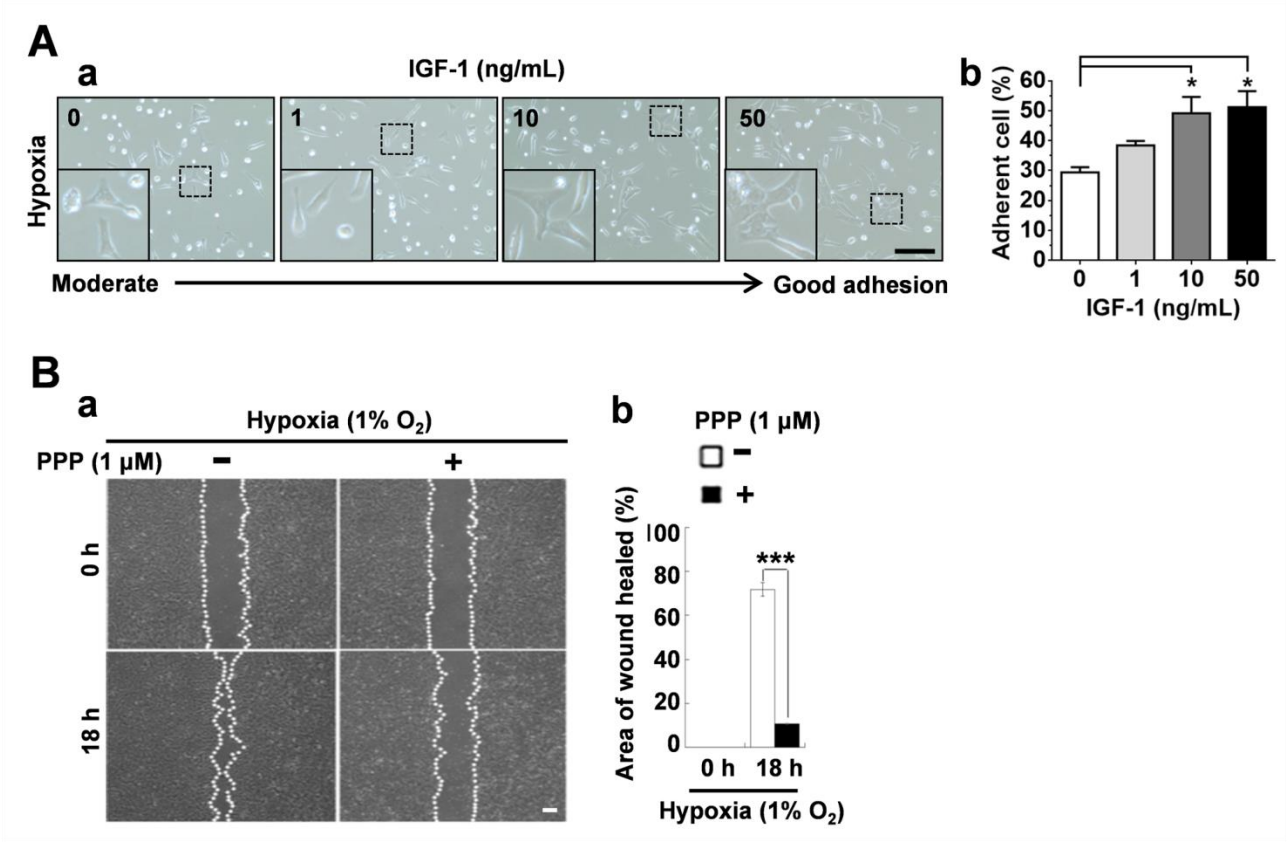

Figure S7. Effect of IGF-1/IGF-1R activation on the cell adhesion and migration of mouse CD49f^{+}AP^{+}GSCs. (Related to main Figures 4 and 5.)

A. Effect of IGF-1 (0, 1, 10, and 50 ng/mL) on the cell morphology of CD49f^{+}AP^{+}GSCs under hypoxia (5% O_2). **(a)** Cell adhesion and morphology. Scale bar, 100 μm. **(b)** Quantitative analysis of **(a)**. Data are the means ± SEM of at least three independent experiments. *P < 0.05. One-way ANOVA. **B.** Migration assay of CD49f^{+}AP^{+}GSCs under hypoxia (1% O_2, 18h) with or without PPP treatment. **(a)** Wound closure assay. **(b)** Quantitative analysis of **(a)**. Data are the means ± SEM of at least three independent experiments. ***P < 0.001. Student's t test. Scale bars, 100 μm.

Supplemental Tables:

Table S1. List of protein classes upregulated in hypoxic AP^{+}GSCs. (Related to main Figure 2)

Protein class	Accession No.	Proportion (%)
Receptor	PC00197	10.9
Extracellular matrix protein	PC00102	10.7
Protease	PC00190	8.4
Cell adhesion molecule	PC00069	6.6
Defense/immunity protein	PC00090	4.8
Calcium-binding protein	PC00060	4.3
Chaperon	PC00072	3.5
Surfactant	PC00212	2.3
Kinase	PC00137	1.8
Ligase	PC00142	1.5
Phosphatase	PC00181	1.0
Membrane traffic protein	PC00150	0.8
Transmembrane receptor regulatory/adaptor protein	PC00226	0.3

Table S2. List of proteins upregulated under hypoxia. (Related to main Figure 2)

Protein	Accession No.	Ratio of Hypo/Normo#	Biological functions and processes
CDH11	Mm.1571	88.42	Calcium ion binding, metal ion binding, cell adhesion, corticospinal tract morphogenesis, etc.
DCN	Mm.56769	29.54	Extracellular matrix binding, glycosaminoglycan binding, regulation of autophagy, etc.
CXCL12	Mm.303231	11.60	CXCR chemokine receptor binding, growth factor activity, chemokine activity, regulation of cell migration, regulation of cell proliferation, germ cell development, etc.
CST3	Mm.4263	6.52	β-amyloid binding, cysteine-type endopeptidase inhibitor activity, identical protein binding, protease binding, response to oxidative stress, regulation of programmed cell death, etc.
LOX	Mm.172	6.32	Oxidoreductase activity, protein-lysine 6-oxidase activity, copper ion binding, metal ion binding, response to steroid hormone, blood vessel development, etc.
CLU	Mm.200608	6.08	Misfolded protein binding, ubiquitin protein ligase binding, intrinsic apoptotic signaling pathway, regulation of cell differentiation, etc.
VEGFA	Mm.282184	5.55	Chemoattractant activity, growth factor activity, VEGF receptor binding, PDGF receptor binding, extracellular matrix binding, angiogenesis, cell differentiation, etc.
MMP2	Mm.29564	5.02	Metalloendopeptidase activity, fibronectin binding, metal ion binding, zinc ion binding, angiogenesis, cell migration, response to hypoxia, embryo implantation, etc.
SPARC	Mm.291442	4.69	Extracellular matrix binding, calcium ion binding, metal ion binding, endothelial cell migration, cell morphogenesis, cell proliferation, cellular response to growth factor stimulus, etc.
CSTB	Mm.6095	4.59	Cysteine-type endopeptidase inhibitor activity, protease binding, negative regulation of proteolysis, etc.
GPC4	Mm.1528	4.57	Heparan sulfate proteoglycan binding.
BGN	Mm.2608	4.36	Extracellular matrix binding, glycosaminoglycan binding, peptide cross-linking via chondroitin 4-sulfate glycosaminoglycan
IGFBP3	Mm.29254	4.09	Insulin-like growth factor binding, fibronectin binding, protein tyrosine phosphatase activator activity, regulation of cell growth, regulation of glucose metabolic process, etc.
THBS2	Mm.26688	3.87	Heparin binding, protein binding, synapse assembly, angiogenesis, cell adhesion.
FBLN2	Mm.249146	3.83	Extracellular matrix binding, protein binding, calcium ion binding, regulation of cell-substrate adhesion.
LAMA1	Mm.303386	3.80	Extracellular matrix structural constituent, receptor binding, glycosphingolipid binding, cell adhesion, cell migration, embryonic development, etc.
CDH2	Mm.257437	3.71	α-, β- ,γ-catenin binding, nitric-oxide synthase binding, phosphatase binding, kinase binding, calcium-dependent cell-cell adhesion, cell migration, neuronal stem cell maintenance, etc.
BMP1	Mm.27757	3.43	Cytokine activity, growth factor activity, metalloendopeptidase activity, protein binding, cartilage development, cell differentiation, multicellular organismal development, etc.
COL4A2	Mm.181021	3.42	Extracellular matrix structural constituent, angiogenesis, etc.
VCAN	Mm.158700	3.32	Carbohydrate binding, hyaluronic acid binding, protein phosphatase binding, cell adhesion, osteoblast differentiation, etc.
COL6A1	Mm.2509	3.22	PDGF binding, cell adhesion, osteoblast differentiation, protein heterotrimerization.
SERPINF1	Mm.2044	3.20	Serine-type endopeptidase inhibitor activity, neurogenesis, angiogenesis, regulation of endothelial cell migration, regulation of inflammatory response, etc.
HSPG2	Mm.273662	3.08	Protease binding, protein binding, metal ion binding, embryonic skeletal system morphogenesis, endochondral ossification, extracellular matrix organization, angiogenesis, etc.
VCL	Mm.279361	3.05	Rho GTPase binding, α-catenin binding, ubiquitin protein ligase binding, adherens junction assembly, lamellipodium assembly, regulation of cell migration, cell-matrix adhesion, etc.

#, The secreted-protein expression levels in hypoxia condition were relative to normoxia condition.

Table S3. Antibody information (Related to main Figures 2, 3, 4, 5, and 6)

WB					
Protein	Cat. No.	Company	Origin	Dilution	Incubation Time
Akt	Sc-8312	Santa Cruz	Rabbit	1:1000	4˚C, overnight
Akt (pSer473)	#9271	Cell signaling	Rabbit	1:1000	4˚C, overnight
c-Kit	Sc-365504	Santa Cruz	Mouse	1:500	4˚C, overnight
Cxcr4	Ab2074	Abcam	Rabbit	1:1000	4˚C, overnight
Cxcr4 (pSer339)	Ab74012	Abcam	Rabbit	1:1000	4˚C, overnight
Hif-2α	NB100-122	NOVUS	Rabbit	1:1000	4˚C, overnight
Igf-1rβ	Sc-713	Santa Cruz	Rabbit	1:1000	4˚C, overnight
Igf-1rβ (pTyr1135/1136)	#3024	Cell signaling	Rabbit	1:1000	4˚C, overnight
Oct4	Sc-5279	Santa Cruz	Mouse	1:500	4˚C, overnight
Stat3	#9132	Cell signaling	Rabbit	1:2000	4˚C, overnight
Stat3 (pTyr705)	#9145	Cell signaling	Rabbit	1:2000	4˚C, overnight
β-Actin	A5441	Sigma-Aldrich	mouse	1:500	4˚C, overnight
ICC					
Arp3	Ab181164	Abcam	Rabbit	1:150	4˚C, overnight
BrdU	M0744	Dako	Mouse	1:200	4˚C, overnight
c-Kit	Sc-365504	Santa Cruz	Mouse	1:100	4˚C, overnight
DAZL	NBP2-23663	NOVUS	Rabbit	1:200	4˚C, overnight
Fak	Sc-1688	Santa Cruz	Mouse	1:50	4˚C, overnight
Fak (pTyr397)	Sc-11765-R	Santa Cruz	Rabbit	1:50	4˚C, overnight
Sdf-1	TP-201	Torrey Pines Biolabs Inc	Rabbit	1:100	4˚C, overnight
Flow Cytometry					
Cxcr4-FITC	#551967	BD Pharmingen	Rat	1:25	4˚C, 90 min
Rat-IgG-FITC	#556923	BD Pharmingen	Rat	1:25	4˚C, 90 min

Table S4. Primer information (Related to main Figures 2 and 3)

Gene	Accession number	Sequence	Size (bp)	Annealing Temp (˚C)
		qRT-PCR		
Sox2	NM_011443	5' GAGTGGAAACTTTTGTCCGAGA 3' 5' GAAGCGTGTACTTATCCTTCTTCAT 3'	151	60
Oct-4	NM_013633	5' TGAAGTTGGAGAAGGTGGAACCAAC 3' 5' CCAAGGTGATCCTCTTCTGCTGCTTCAG 3'	111	60
Hif-2α	NM_010137	5' AGCTTCAGATTCATTTTCAGAGCA 3' 5' CCTTCGGACACATAAGCTCCTG 3'	54	60
Nanog	NM_028016	5' CCTGTGATTTGTGGGCCTG 3' 5' GACAGTCTCCGTGTGAGGCAT 3'	78	60
Sdf1-α	NM_021704	5' CGCTCTGCATCAGTGACGGTA 3' 5' GTTCTTCAGCCGTGCAACAATC 3'	152	60
Igf-1rβ	NM_010513	5' GGAGTGTCCCTCAGGCTTCA 3' 5' CATCGCCGCAGACTTTGG 3'	88	60
Cxcr4	NM_009911	5' AGCCTGTGGATGGTGGTGTTTC 3' 5' CCTTGCTTGATGACTCCCAAAAG 3'	242	60
Igf-1	NM_010512	5' AAGCAGCCCGCTCTATCC 3' 5' TTCTGAGTCTTGGGCATGTCA 3'	55	60
Cdh11	NM_009866	5' TCTTCTGGTCATCGTTGTGC 3' 5' AGGGTGGCTATGTCGAAGG 3'	156	60
Lox	NM_010728	5' GACATTCGCTACACAGGACATC 3' 5' CCAGGTACGGCTTTATCCAC 3'	98	60
Vegfa	NM_001025250	5' GACGGGCCTCCGAAACC 3' 5' GCAGCCTGGGACCACTTG 3'	97	60
Igfbp-3	NM_008343	5' TCAAAGCACAGACACCCAGAAC 3' 5' GATGATTCAGTGTGTCCTCCATTTC 3'	95	60
Lama1	NM_008480	5' CAGAGACCTTGAAAATGTTAGAAACG 3' 5' TCGGAGATCAAGTCTGTCTTATTCG 3'	147	60
Col4a2	NM_009932	5' AGTGGGTACAGCCTGCTATATTTTG 3' 5' CCGGATTGCAGTACAGGAAAG 3'	118	60

β-2m	NM_009735	5’ CCGAACATACTGAACTGC 3’	185	60
		5’ AGAAAGACCAGTCCTTGC 3’		
		Methylation Specific PCR and Pyrosequencing		
Dppa3	NM_139218	5’ GGTGGTTATTATTGTTAGGTTTGAAGT 3’		
		5’ ACCCAATCTACCCCCAAACTACTTTA 3’		
		Pyro seq. 5’ GGAATTGGTTGGGAT 3’		
Ddx4	NM_001145885	5’ GAATTGATGAGTTTTTGGAGAGAGAA 3’		
		5’ ACCTCTCCCCTCCAAACTCCCC 3’		
		Pyro seq. 5’ GGTTTAGGTTTTAATAAAGGTGG 3’		
Nanog	NM_028016	5’ GGATTTTGTAGGTGGGATTAATTG 3’		
		5’ CGCCAGGGTTTTCCCAGTCACGACCTACCCTACCCACCCCCTATTCT 3’		
		Pyro seq. 5’ TGAATTTATAGGGTTGGTG 3’		
Oct4	NM_013633	5’ TTAAGGTTAGAGGGTGGGATTG 3’		
		5’ CGCCAGGGTTTTCCCAGTCACGACTCTAAAACCAAATATCCAACCATA 3’		
		Pyro seq. 5’ GGAGGGAGAGGTGAAAT 3’		
Prdm14	NM_001081209	5’ GTTTAGGTTTAGGGAGGGTAGAATGTA3’		
		5’ CCCTTTAAAACCCCATAAACTAATTCT 3’		
		Pyro seq. 5’ AGGGTAGAATGTATTGTT 3’		

1

Supplemental Experimental Procedures:

Alkaline phosphatase activity assay

Clumped germline stem cell (GSC) colonies cultivated under 21%, 5%, 3%, or 1% O_2 atmosphere were fixed with 4% paraformaldehyde for 30 min at room temperature. The alkaline phosphatase (AP) activity of these GSCs was examined using an AP detection kit (Chemicon, Hampshire, UK), and Nitro Blue Tetrazolium/ 5-Bromo-4-chloro-3-indolyl phosphate (NBT/BCIP) substrate (Sigma-Aldrich, St. Louis, MO, USA) according to the manufacturer's instructions.

Identification of protein expression profiles using LC-MS/MS and the Mascot Distiller search engine

Peptide mixtures obtained from the conditioned medium of AP^+GSC colonies cultivated under 21% O_2 (normoxia control) and 5% O_2 (hypoxia) was separated using a BioBasic C_{18} column (150 mm × 2.1 mm, particle size 5 μm) with a gradient from 5% to 70% acetonitrile in 0.1% formic acid over 90 min at a flow rate of 200 μL/min. The MS/MS analysis was performed using a LTQ Velos system (Thermo Fisher Scientific) in the positive electrospray ionization mode with a survey scan for the precursor ion that ranged from m/z = 400–1600. The MS/MS raw data acquired from either the control or hypoxia-treated sample were processed into an MGF file using Mascot Distiller v2.3.2.0 (Matrix Science, London, UK). The resulting MGF files of the control or hypoxia-treated samples were searched using the Mascot search engine v2.3 (Matrix Science) with the following search parameters: (1) the protein database was set to Swiss-Prot; (2) the taxonomy was set as *Mus musculus* (house mouse); (3) one trypsin missed cleavage was allowed; (4) the precursor and product ion mass tolerance were set to 1.20 Da and 0.60 Da, respectively; (5) carbamidomethyl (C) was chosen for fixed modification; (6) oxidation (M) was chosen for the variable modification; and (7) the significance threshold was $P < 0.05$. The relative quantitative analysis of protein expression in the control or hypoxia-treated samples was performed using Mascot Distiller v2.3.2.0 and the label-free quantitation mode. The parameters of the Mascot Distiller were set as follows: (1) report ratio: C1/Ref (C1 and Ref represent hypoxia-treated and control samples, respectively); (2) protocol: replicate; (3) integration method: Simpson's; (4) integration source: survey (precursor peak area from survey scan); (5) correlation threshold: 0.6; (6) Std. Err. threshold: 999 (threshold on the standard error for a straight line fit of the component intensities from each of the scans in the XIC peak); (7) XIC threshold: 0.1; (8) max XIC width (upper limit on the number of survey scans in an XIC peak): 250; (9) XIC smoothing: 3; (10) peptide threshold type: at least identity; and (11) outlier method: auto (using Dioxon's or Rosner's outlier method according to the number of values). The relative quantitation result was then normalized using the ratio of the internal standard (β-ACTIN).

Trypsin digestion of proteins extracted from PGC-like AP^+GSCs with and without hypoxia treatment

Either hypoxia-treated or control PGC-like AP^+GSCs proteins (100 μg) dissolved in deionized water (60 μL) were denatured and reduced at 95°C for 5 min using 7.5% SDS (9.3 μL) and 1M 1,4-dithiothreitol (0.7 μL). Subsequently, 0.5 M iodoacetamide (8 μL) was added to the protein mixture, which was then incubated at room temperature in the dark for 30 min. Afterward, 50% trichloroacetic acid (52 μL) was added and the precipitate was washed with deionized water (200 μL × 3). The resulting protein precipitate was dissolved in 50 mM ammonium bicarbonate (100 μL) and 2%

N-octyl-β-D-glucopyranoside (5 μL). Sequencing-grade trypsin (2 μg) was added and the mixture was incubated at 37°C for 18 h. The resulting tryptic digest was acidified with 2% formic acid (10 μL) to stop the enzymatic reaction, and the resulting digest was lyophilized and maintained at -20℃.

Gene ontology (GO) analysis

The differential protein secretion profiles of mouse AP^+GSCs were analyzed by the PANTHER classification system (Mi et al., 2016) for gene ontology secretome analysis. Four selected items of the signaling pathway category were pluripotency regulation of stem cells (KEGG pathway map No.: mmu04550), PI3K-AKT signaling pathway (mmu04151), Chemokine-associated signaling pathway (mmu04512), and HIF signaling pathway (mmu04066). STRING program (Szklarczyk et al., 2015) was used for protein network analysis.

RNA extraction, reverse transcription, and quantitative real-time polymerase chain reaction

The AP^+GSC colonies and $CD49f^+AP^+$GSC cultivated under 21% and 5% O_2 atmosphere were collected. Total RNA was extracted using the Trizol Kit (Invitrogen, Frederick, MD, USA), and complementary DNA was synthesized using Moloney murine leukemia virus reverse transcriptase (Thermo Fisher Scientific) according to the manufacturer's instructions. Quantitative real-time polymerase chain reaction (qRT-PCR) was performed using the FastStart Universal SYBR Green Master Mix (Roche, Indianapolis, IN, USA) in a LightCycler 480 instrument (Roche), and the qRT-PCR results were recorded and analyzed using the instrument's application software. Gene expression levels were normalized by *β-2 microglobulin* (*β-2m*). Primer sequences are listed in Table S4.

Transcriptome analysis

Total RNA was extracted from the E11.5 PGC colony, P2 AP^+GSC colony, and $CD49f^+AP^+$GSCs using the Trizol reagent (Invitrogen). The quality of the total RNA was assessed using an Agilent 2100 Bioanalyzer (Agilent Technologies, Santa Clara, CA, USA). Fluorescent aRNA targets were prepared from 1 μg of total RNA samples using a OneArray® Amino Allyl aRNA Amplification Kit (Phalanx Biotech Group, Hsinchu, Taiwan) and Cy5 dye (GE Healthcare). Fluorescent targets were hybridized to a Mouse Whole Genome OneArray® with Phalanx hybridization buffer using the Phalanx Hybridization System. The Mouse Whole Genome OneArray® v2 (Phalanx Biotech Group) contains 27,307 DNA oligonucleotide probes. Among the probes, 26,423 correspond to the annotated genes in the RefSeq v42 and Ensembl v59 databases. In addition, 884 control probes are included. Briefly, after hybridization and washing, the slides were scanned using a DNA Microarray Scanner (Model G2505C, Agilent Technologies). The Cy5 fluorescent intensity of each spot was analyzed using the GenePix 4.1 software (Molecular Devices). Each single sample was analyzed at least twice in terms of technical or biological replicates, with a reproducibility of more than 0.975. The signal intensity was loaded into the Rosetta Resolver System® (Rosetta Biosoftware, WA, USA) to perform data preprocessing and applied to a 75 percentile centering normalization. The errors of the sample were estimated using an error-weighted approach simultaneously. Both the fold change and *P* value for the pair-wise sample comparison were calculated to evaluate the differentially expressed genes. A fold change of ≥ 2 or ≤ -2 and a *P* value of <0.05 are strongly recommended for further analysis.

Bisulphite conversion, methylation-specific PCR, and pyrosequencing

Total genomic DNA was isolated from the E11.5 PGC colony, P2 AP^+GSC colony, and $CD49f^+AP^+$GSCs. First, 500 ng of genomic DNA was bisulphite-converted using the EpiTect Fast bisulphite conversion kit according to the manufacturer's instructions (QIAGEN, Germantown, MD, USA). Bisulfate Specific PCR was performed using a PyroMark PCR kit (QIAGEN), followed by PCR product purification. The purified PCR product was hybridized with a pyrosequence primer using PyroMark Gold Q24 reagent according to the Pyromark Q24 vacuum workstation guide (QIAGEN). The methylation percentage per CpG position was determined using the PyroMark Q24 software (QIAGEN). Briefly, the methylation percentage was assessed by the ratio of real-time incorporated C and T nucleotides into the growing DNA strand, resulting in an enzymatic cascade of pyrophosphate release and the production of a light signal. *Nanog* and *Oct4* pyrosequence primer information was according to a study conducted by Rugg-Gunn et al. (2010). Primer sequences are listed in Table S4.

Flow cytometry

For the hypoxia experiment, $CD49f^+AP^+$GSCs were cultivated under 1%, 5%, or 21% O_2 atmosphere for 3 days. For the flow cytometry analysis of cell surface CXCR4, the culture medium was replaced every day to eliminate the secreted SDF-1 in the medium, which may lead to cell surface CXCR4 internalization (Signoret et al., 1998). For the IGF-1R signaling inhibition experiment, the cells were treated with or without the IGF-1R phosphorylation inhibitor cyclolignan picropodophyllin (PPP, 1 μM, Enzo Life Sciences, Farmingdale, NY, USA) under 1% O_2 atmosphere for 3 days. Cells were detached using Accutase® treatment (Innovative Cell Technologies, San Diego, CA, USA), followed by immunostaining with antibodies against specific surface markers for flow cytometry analysis. Briefly, 2×10^5 cells were incubated with 1% BSA/PBS blocking solution for 30 min and then interacted with a fluorescein isothiocyanate-conjugated CXCR4 antibody or isotype control (BD Pharmingen, San Jose, CA, USA) at 4℃ for 90 min. After resuspension in PBS buffer, the $CXCR4^+$ cell percentage was analyzed using a BD FACSVerse cytometer and the instrument's application FACSuite software (BD Biosciences, San Jose, CA, USA). The primary antibodies used in the experiment are listed in Table S3

Western blot analysis

For oxygen tension experiments, $CD49f^+AP^+$GSCs were cultivated under 1%, 5%, or 21% O_2 atmosphere for 3 days; for IGF-1 experiments, the cells were treated with IGF-1 (0–50 ng/mL, PeproTech, Rocky Hill, NJ, USA) under 21% O_2 for 3 days. For HIF-2α knockdown experiments, the cells were transfected with a high-efficiency shHIF-2α clone (NM_010137, 5'-ggagacggaggtcttctat-3') (Huang et al., 2014) or shCtrl (TRCN0000072246, National RNAi Core, Taiwan) for 24 h and then treated with or without IGF-1 (10 ng/mL) for an additional 24 h. For receptor crosstalk experiments, the cells were pretreated with or without PPP (1 μM) or AMD3100 (50 μM, Sigma-Aldrich) for 6 h and then treated with IGF-1 (50 ng/mL) or SDF-1 (400 ng/mL, PeproTech) for 0, 2, and 5 min. The cell lysates of $CD49f^+AP^+$GSCs were collected and extracted using reducing 2× Laemmli sample buffer and subjected to 10% SDS-PAGE electrophoresis; western blotting analysis was then performed. The primary antibodies used in the experiments are listed in Table S3, and horseradish peroxidase-conjugated anti-mouse or anti-rabbit IgG (1:2000) served as the secondary antibody. HRP enzyme activity was detected using an enhanced chemiluminescence system

according to the manufacturer's instructions (Amersham Pharmacia Biotech, Buckinghamshire, UK). Quantifications of the protein bands were performed using the SPOT DENSO software on an AlphaImager2200 instrument (Alpha Innotech Corporation, CA, USA).

Immunocytochemical staining

For the BrdU incorporation assay, GSC colonies were cultivated under 5% O_2 atmosphere at 37℃ for 7 days, and BrdU (0.1 mM) was added to the medium for further 24 h incubation. Excess BrdU in the medium was removed by three washes with PBS, and the BrdU-incorporated cells were fixed with 4% paraformaldehyde and treated with 2 N HCl, followed by neutralization with 0.1 M sodium borate. For hypoxia experiments, $CD49f^+AP^+$GSCs were cultivated under 1%–21% O_2 atmosphere for 3 days, and AP^+GSCs were cultivated under a 5% O_2 atmosphere for 7 days; for PPP inhibition experiments, the cells were treated with or without PPP (1 μM) under 1% O_2 oxygen concentration for 3 days. All experiments were performed using immunocytochemical analysis. Cells were fixed in 4% paraformaldehyde, permeabilized with 0.5% triton X-100 in PBS, and then blocked with 3% BSA in 0.5% triton X-100 in PBS. Cells were incubated with a primary antibody (Table S3) at 4℃ overnight and then interacted with Alexa 488- or Alexa 594-conjugated secondary antibodies (Invitrogen). The nuclei of all cells were counterstained with 4',6-diamidino-2-phenylindole (Sigma-Aldrich) and analyzed using a fluorescence microscope (Leica, Buffalo Grove, IL, USA) or a laser confocal microscope (Leica).

Migration assay and wound healing assay

Transwell assays were performed using an 8-μm pore transwell insert in 24-well plates (Corning, Corning, NY, USA). The upper chambers were seeded with $CD49f^+AP^+$GSCs (1.5×10^5/100 μL), followed by treatment with IGF-1 (0–50 ng/mL) in lower chambers as an attractant for 3 days. For hypoxia experiments, the PPP groups of $CD49f^+AP^+$GSCs were pretreated with PPP (1 μM) for 2 h. All experimental cells were treated with PPP (1 μM) or SDF-1 (100 ng/mL) in the upper chamber and then treated with IGF-1 (50 ng/mL) in the lower chamber under 21%, 5%, and/or 1% O_2 atmosphere for 3 days. Migrated cells were stained with crystal violet and counted in six random fields under a light microscope. For the wound healing assay, $CD49f^+AP^+$GSCs (1×10^5/well) were seeded into a culture insert (Ibidi, Martinsried, Germany). Adherent cells were treated with IGF-1 (50 ng/mL), SDF-1 (100 ng/mL), or PPP (1 μM) under different culture conditions. At the end point, cells were stained with crystal violet. The photos of the cells were taken at each time point, and the gap area was measured and quantified.

Supplemental References:

Huang, Y.H., Lin, M.H., Wang, P.C., Wu, Y.C., Chiang, H.L., Wang, Y.L., Chang, J.H., Huang, Y.K., Gu, S.Y., Ho, H.N. et al. (2014). Hypoxia inducible factor 2alpha/insulin-like growth factor receptor signal loop supports the proliferation and Oct-4 maintenance of mouse germline stem cells. Mol Hum Reprod. *20*, 526-537.

Mi, H., Poudel, S., Muruganujan, A., Casagrande, J.T., Thomas, P.D. (2016). PANTHER version 10: expanded protein families and functions, and analysis tools. Nucleic Acids Res. *44*, D336-342.

Rugg-Gunn, P.J., Cox, B.J., Ralston, A., Rossant, J. (2010). Distinct histone modifications in stem cell lines and tissue lineages from the early mouse embryo. Proc Natl Acad Sci U S A. *107*, 10783-10790.

Signoret, N., Rosenkilde, M.M., Klasse, P.J., Schwartz, T.W., Malim, M.H., Hoxie, J.A., Marsh, M. (1998). Differential regulation of CXCR4 and CCR5 endocytosis. J Cell Sci. *111 (Pt 18)*, 2819-2830.

Szklarczyk, D., Franceschini, A., Wyder, S., Forslund, K., Heller, D., Huerta-Cepas, J., Simonovic, M., Roth, A., Santos, A., Tsafou, K.P. et al. (2015). STRING v10: protein-protein interaction networks, integrated over the tree of life. Nucleic Acids Res. *43*, D447-452.